R. & M. No. 3593

MINISTRY OF TECHNOLOGY

AERONAUTICAL RESEARCH COUNCIL

REPORTS AND MEMORANDA

Tests at Subsonic and Supersonic Speeds on a Slender Cambered Wing with Fin, Underwing Engine Nacelles and Trailing-Edge Controls

By D. ISAACS

Aerodynamics Dept., R.A.E., Bedford

LONDON: HER MAJESTY'S STATIONERY OFFICE

1969

PRICE £1 4*s.* 6*d.* NET

Tests at Subsonic and Supersonic Speeds on a Slender Cambered Wing with Fin, Underwing Engine Nacelles and Trailing-Edge Controls

By D. ISAACS

Aerodynamics Dept., R.A.E., Bedford

Reports and Memoranda No. 3593*
September, 1967

Summary.

The tests were made in the 8 ft × 8 ft wind tunnel at R.A.E. Bedford on a 1/36 scale model of a possible design for a supersonic transport aircraft. The wing camber was designed, using slender-wing theory, to have attached flow at a C_L of 0·02, and a shift forward of the centre of pressure, relative to the uncambered wing, of 0·3 $\bar{c}$ at $C_L = 0{\cdot}1$.

The present investigation was restricted to determining the effects of the fin and nacelles on the longitudinal stability, drag, and lateral stability of the wing and to measurements of effectiveness, drag, and hinge moment of the controls.

*Replaces R.A.E. Tech. Report No. 67217 (A.R.C. 30 070).

LIST OF CONTENTS

---

1. *Introduction.*

Tests have been made in the 8 ft × 8 ft tunnel on a model which represented a possible layout for a supersonic transport aircraft (Bristol type 198). The model was of 1/36 scale, and identical to one of a series of seven smaller scale (1/90) models (500 series)[1], which had been designed to investigate various area distributions and camber shapes. The design philosophy behind these models has been put forward in Ref. 1, but it may be helpful to give a summary of the important details here. Three of the seven models were uncambered, and of these, one was a datum wing-body combination with the body designed simply on full scale payload requirements with no attempt at minimisation of drag. The other two uncambered models featured body waisting, and in one case the nose was lengthened to shift the centre of gravity of the full scale aircraft forward, and so ease the trimming problem. Of the four cambered models, three were designed by linear theory at $M = 2{\cdot}2$ with various combinations of design C_L and centre-of-pressure shift, and using the lengthened body with optimised area distribution. The model, which is the subject of these tests, was identical to the remaining cambered model, which used the unlengthened body with optimised area distribution. The camber was designed by slender-wing theory so that the wing would have attached flow at a C_L of 0·02, and a stable separated flow over the upper surface at the cruise C_L of 0·1. At the cruise C_L the forward centre-of-pressure shift (relative to the uncambered wing) was designed to be 0·3 $\bar{c}$. Previous experience with wing camber designed by slender-wing theory[2] has shown that approximately only half the design centre-of-pressure shift is realised at $M = 2{\cdot}2$, so that the present model has been designed intentionally for a larger centre of pressure shift than is necessary to trim at $C_L = 0{\cdot}1$ and $M = 2{\cdot}2$.

In previous designs[2,3] there have been varying degrees of integration between wing and body, and the body volume has usually been added symmetrically above and below the wing camber line. With the present series of designs there is no attempt at integration and asymmetric distribution of body volume is accepted.

The longitudinal stability and drag of the present model without fin or nacelles and with undeflected controls (defined here as the basic wing-body) has been investigated by Cook[4], and the present tests are concerned with the measurement of the lateral stability of the basic wing-body, the effectiveness, drag, and hinge moment of the trailing-edge controls, and the effect on longitudinal stability, drag, and lateral stability of adding a stabilising fin and underwing engine nacelles.

2. *Experimental Details.*

2.1. *Description of the Model.*

The wing leading edge has constant sweepback (68°) over most of the span and is smoothly faired into streamwise tips. The trailing edge is unswept (Fig. 1). At the intersection of the wing leading edge and the body, the wing blends smoothly into a triangular cross-section strake which extends forward to the nose of the model, thus giving a sharp leading edge from nose to tail (Fig. 2). Clearly shown in Fig. 2 is the leading-edge droop of the wing, intended to maintain attached flow at the design C_L, and the asymmetric distribution of body volume about the wing camber line. Details of the chordwise camber relative to the OH datum of both wings and body are shown in Fig. 3. The OH datum, which is also shown as a reference datum in Figs. 1 to 5, is aligned in the direction of the free stream when the aircraft is at its design attitude (design $C_L = 0{\cdot}02$). The OV datum is simply the aircraft centreline.

The engine nacelles are of near rectangular cross-section with scalloped undersurfaces, and are mounted in an underwing location between the inboard and outboard trailing-edge controls (Fig. 4). In order to obtain the correct external flow and internal mass flow at the design Mach number ($M = 2{\cdot}2$), a constant area duct was provided through the nacelle.

The planform details of the controls are shown in Fig. 4. Both controls are hinged at their leading edges, the outboard control having a horn type aerodynamic balance projecting ahead of the hinge line. On the port wing, each control is supported from the wing at the hinge line by two strain-gauged beams, which are entirely enclosed within the wing contour. In addition to measuring the control hinge moment, these beams serve to set the control at the required angle; thus it was necessary to manufacture and strain gauge two beams per control for each control setting. The controls on the starboard wing are identical to

those on the port wing except that the beams are not strain gauged. The hinge-line gaps were sealed for all the tests.

Apart from the control hinge moments, all model forces and moments were measured on a six-component internal strain-gauge balance supported by a sting. It was necessary to distort the rear of the model in order to accommodate the sting, the distortion taking the form of a cylindrical shroud which for the majority of tests ended at the wing trailing edge (Fig. 5). For the tests with the fin on, a longer shroud was used, the shroud also serving as a suitable mounting for the fin. The fin is of cropped 'double-delta' planform and 6 per cent thick biconvex section outboard of the kink in the leading edge. Inboard of the kink, the biconvex section is modified by a single wedge extension which blends into the biconvex section ahead of the point of maximum thickness. The fin shape and location are correctly representative of full scale, so that a small area of the fin near the root is shielded by the sting shroud (Fig. 5).

Fig. 6a shows the area distribution of the basic wing-body non-dimensionalized with respect to the total length, L, and the effects on this of the sting shroud, the fin, and the nacelles. The component area distributions of the fin and one nacelle are also shown separately in Fig. 6b. The cross-section area of the nacelle is taken to be the total cross-section area of the nacelle less the stream tube entry area at the cowl lip.

The full scale aircraft was designed to have a variable geometry canopy. In the supersonic configuration the only effect the canopy has on the fuselage profile is a small step on the upper surface of the nose at 13·4 per cent L, just noticeable in Fig. 1. For take off and landing the upper surface profile ahead of the canopy would retract into the fuselage to improve the pilots' view. Although the present model was tested at subsonic speeds ($M = 0{\cdot}275$) there was no provision for varying the canopy geometry and the supersonic configuration was tested throughout.

The main part of the model (aft of 50 per cent L), including the nacelles, was made of steel with the nose and fin constructed of glass fibre and epoxy resin on steel cores.

The principal dimensions of the model, and the setting angles of unloaded controls are given in Tables 1 and 2 respectively.

2.2. *Test Conditions.*

The majority of tests on this model were made at supersonic speeds, at Mach numbers of 1·4, 1·8 and 2·2. For the tests on the configuration with engine nacelles $M = 1{\cdot}4$ was omitted. The range of sting incidences covered by the tests was from $-4°$ to $+12°$, and for the basic wing-body, the wing-body with fin, and the wing-body with nacelles, lateral components were measured at sideslip angles of $-2°$ to $+6°$ at selected incidences. In addition to the above tests at supersonic speeds, the basic wing-body and the wing-body with fin were tested at $M = 0{\cdot}275$ at incidences of 0° to 20° and sideslip angles of $-2°$ to $+6°$.

At all Mach numbers the Reynolds number was 2×10^6 per foot (approximately 6×10^6 based on root chord, c_0).

All other details of the test programme are given in Table 3.

Bands of distributed roughness (carborundum grains with an effective height of between 0·008 and 0·012 inches) were applied to the leading edges of the wing, fin, and nacelles and the body nose in order to produce a turbulent boundary layer over the model.

2.3. *Corrections Applied to Results.*

Each configuration has been tested with the model both 'upright' and 'inverted' in the tunnel airstream, and the results presented in this note are a mean of these two sets of measurements. This procedure eliminates from the results any effects of flow deflection or flow curvature, apart from the effect of flow curvature on drag.

The model attitude has been corrected for deflections of the balance and sting, and the trailing-edge control setting angles have been corrected for deflection of the support beams.

A tunnel constraint correction has been applied to the model incidence, drag, and pitching-moment

coefficients at $M = 0{\cdot}275$. The corrections were derived from the theory of Ref. 5 and the corrected values are given by:

$$\alpha \text{ correct} = \alpha + 0{\cdot}579\, C_L \tag{1}$$

$$C_D \text{ correct} = C_D + 0{\cdot}00810\, C_L^2 \tag{2}$$

$$C_m \text{ correct} = C_m + 0{\cdot}00132\, C_L \tag{3}$$

where α (in degrees), C_L, C_D, and C_m are the uncorrected values.

Although the axial force measurements have been corrected for the difference between the base pressure and free-stream static pressure, no other corrections for the presence of the sting shroud have been applied to the results.

The drag results of the configuration with nacelles have been corrected to allow for the internal drag of the nacelles. The location of the nacelles on the present model is such as to allow several possible definitions of internal drag, dependent upon the location of the upstream reference plane. The correction applied to the present drag results is that for the upstream reference plane located at the apex of the intake sideplates at $0{\cdot}785\, L$ or 2·5 per cent ahead of the cowl lip. The correction was determined from the results of two pressure surveys, one over the region of duct inlet with the nacelle removed and the other over the duct exit with the nacelle in position. Pitot pressures were measured on the starboard wing and static pressures on the port wing. The most usual alternative form of the correction to the present one is with the upstream reference plane in the free stream, and both the above forms of the correction are shown in Fig. 7. The two forms of the correction are only significantly different at negative incidence. Over most of the incidence range the difference between them is of the same order as the experimental accuracy (*see* section 4). The correction to pitching moment is negligible and has been ignored. No measurements of nacelle internal flow were made with the wing yawed, so that it was not possible to determine any corrections to yawing moment.

3. *Presentation of Results.*

The usual coefficient form of presentation of model forces and moments is used throughout (*see* list of symbols), and unless otherwise stated the coefficients refer to a stability system of axes. The moment reference centre is at 50 per cent $\bar{c}$ (12·305 inches forward of the trailing edge). The tangent definition of incidence (α) and the sine definition of sideslip (β) is used throughout:

$$\tan\alpha = \tan\theta\cos\phi \tag{4}$$

$$\sin\beta = \sin\theta\sin\phi \tag{5}$$

where θ is the total incidence and ϕ is the roll angle from the trailing edge horizontal. Unless otherwise stated the model incidence is measured relative to the wing root chord (*see* Table 1).

Because of the duplication of experimental points by taking measurements with the model both 'upright' and 'inverted', only the mean faired curves are shown in the figures, the experimental points being omitted in the interests of clarity.

4. *Accuracy of Results.*

At supersonic speeds the absolute experimental accuracy of the meaned results is estimated to be:

C_L $\pm 0{\cdot}002$

C_m $\pm 0{\cdot}0002$

C_D $\pm 0{\cdot}0002$

C_Y $\pm 0{\cdot}001$

C_n $\pm 0{\cdot}0002$

C_l $\pm 0{\cdot}0004$

C_H $\pm 0{\cdot}002$.

At $M = 0{\cdot}275$ due to the low kinetic pressure the above values should be doubled. The accuracy of differences is probably slightly better than the above figures.

An unpublished flow survey has shown that the Mach number variation over the region of the model is within the following limits:

M_{nominal}	*Variation*
0·275	$\pm 0{\cdot}001$
1·4 to 2·2	$\pm 0{\cdot}005$.

Model incidence and sideslip angles and control setting angles are all accurate to $\pm 0{\cdot}03$ deg.

5. *Discussion of Results.*

The analysis of the longitudinal stability and drag results for the basic wing-body is given elsewhere[4] and will not be discussed here.

5.1. *Effect of Fin and Nacelles on Longitudinal Stability and Drag.*

At $M = 0{\cdot}275$ the effect of the fin on lift, pitching moment and drag is small (Figs. 8, 9 and 10), and in view of the relatively large values of C_L and C_D which would be experienced by an aircraft at take off and landing ($C_L \simeq 0{\cdot}50$, $C_D \simeq 0{\cdot}11$), is of little concern.

At supersonic speeds where the cruise C_L is relatively small (0·1) the effect of the fin is more significant. At low incidence addition of the fin produces a small decrease in C_L, whereas at high incidence this is partly or wholly offset by a slight increase in lift-curve slope with the fin present (Fig. 11). This latter effect is probably due to the extra length of sting shroud which is capable of taking carry-over lift from the wing. The nacelles give an increase of lift at all incidences. The different sense of the lift increment at low incidences resulting from the addition of fin and nacelles is due entirely to the location of these components, above and below the wing respectively.

At zero C_L the effects on C_m of fin and nacelles are consistent with their respective lift increments and locations (Fig. 12). Adding the fin produces a nose-up change in C_m whereas the nacelles give a nose down change. In both cases a slight rearward movement of aerodynamic-centre position occurs. In the case of the nacelles this may well be due to the additional plan area located behind the wing trailing edge (Fig. 4). With the fin, the aerodynamic-centre movement is probably not a genuine fin effect but due to the extra length of sting shroud, which was inferred to be the cause of the increased lift-curve slope with this configuration. The full scale body radius aft of the trailing edge is much less than that of the sting shroud (Fig. 5) and consequently will support much less carry-over lift, and in addition, the contracting afterbody will develop some negative lift which will move the aerodynamic-centre position forwards, so that its true location 'fin on' may well be further forward than indicated by Fig. 12.

Fig. 13 shows the effect of fin and nacelles on the drag polar.

5.1.1. *Incremental loads due to fin and nacelles.* The incremental values of C_L and C_m at $\alpha = 2{\cdot}90°$ (wing trailing edge at zero incidence) due to the fin have been replotted in Fig. 14a and b.

Using linear theory, Jones[6] has calculated the lift and pitching moment produced at supersonic speeds by a delta fin of biconvex section mounted on a flat wing with unswept trailing edge. The only restriction imposed in Ref. 6 on fin location was that the Mach line from the fin root leading edge should not intersect the wing leading edge. Using the charts of Ref. 6 and a simplified model of the fin, shown in Fig. 15, an attempt has been made to estimate the lift and pitching moment produced by the present fin. The wing was assumed to be flat and the sting shroud and body were ignored. Initially the lift and pitching moment were determined for a delta fin of 58° 33′ leading edge sweepback located with its trailing edge in the same

position as that of the present fin (Fig. 15). A correction to allow for the dorsal extension of the present fin was then obtained by assuming that the additional fin volume could be represented by a delta fin of 79° 18′ leading edge sweepback and biconvex section with its trailing edge situated 10·295 inches ahead of the trailing edge of the present fin. The accuracy of prediction is not very good (Fig. 14a and b), the measured values of ΔC_L and ΔC_m due to the fin being smaller than the theoretical values. Since the cropped tip of the fin lies behind the wing trailing edge it cannot influence the induced lift and pitching moment, so that the main sources of error in the prediction are the effect of the dorsal extension on the pressure field from the main part of the fin, and the effect of the sting shroud extension in carrying additional induced load aft of the wing trailing edge. The sense of this additional induced load is almost certainly such as to increase C_L and decrease C_m which could account for the disparity.

The contribution of skin friction to the drag increment of the fin was calculated by determining the skin-friction drag of a series of chordwise strips and integrating these across the span of the fin. The boundary layer was assumed to be turbulent from the fin leading edge, and the skin-friction coefficient of each strip was calculated by the intermediate enthalpy method using the Prandtl-Schlichting formula.

Estimates of the fin wave drag were obtained from the charts of standard methods. A simplified planform shape was assumed, with the forward part of the double-delta planform being ignored. These estimates of fin drag coefficient are shown in Fig. 14c in comparison with the measured drag-coefficient increment due to the fin. At both subsonic and supersonic speeds there is evidence of favourable interference between wing and fin, the measured drag coefficients being much lower than predicted.

The increments in C_L and C_m at $\alpha = 2{\cdot}9°$ and in minimum C_D, due to the nacelles, are shown in Fig. 16. The skin friction drag coefficient of the nacelles, shown in Fig. 16c, was estimated as the skin-friction drag of the external wetted area of the nacelle under the wing, less the skin-friction drag of the wing covered by the nacelles (from apex of intake sideplates to wing trailing edge), plus the small additional skin-friction drag of the upper surface of the nacelles projecting beyond the wing trailing edge. The method of estimation of the skin-friction drag coefficient was identical to that for the fin, except that here it was considered accurate enough to base the skin-friction coefficients on the mean Reynolds numbers involved rather than perform integrations. Simple estimates of nacelle wave-drag coefficients were obtained from the charts of standard methods. The nacelle area distribution was used to calculate an equivalent quasi-cylindrical half-body of revolution having a parabolic profile. The estimated drag-coefficient increment is much lower than measured (Fig. 16c). Although the wave-drag estimate is very approximate, it is not likely to be in error by the amount shown in Fig. 16c so that there would appear to be a significant amount of unfavourable interference.

5.2. *Trailing-Edge Controls.*

Deflection of the trailing-edge controls as elevators has only a small effect on lift-curve slope (Figs. 17 and 20a) or aerodynamic-centre position (Figs. 18 and 21a), so that the increments in C_L and C_m are virtually independent of α and C_L respectively. The increase in C_D due to deflecting the controls as elevators is shown by Figs. 19 and 22a. Differential movement of the outboard controls (as ailerons) has no effect on C_L or C_m (Figs. 20b and 21b respectively), and the increase in C_D is shown by Fig. 22b. The rolling-moment coefficient increment due to a constant aileron angle decreases slightly with increasing incidence (Fig. 23). At $\alpha = 2{\cdot}90°$, where the wing trailing edge is horizontal (*see* Table 1), the increments in C_L, C_m and C_l vary linearly with control-setting angle within the range of setting angles tested (Figs. 24, 25 and 26).

5.2.1. *Control effectiveness.* The supersonic linear-theory solutions for $dC_L/d\eta_c$ and $dC_m/d\eta_c$ of a rectangular control in an inboard location are given in Ref. 7, and a method for correcting this linear-theory solution for control-thickness effects is suggested by Tucker and Nelson in Ref. 8. Although this correction applies strictly only to rectangular planform or two-dimensional wings, an analysis of hinge moments on rectangular controls[9] showed that the experimental correlation was improved when this thickness factor obtained from Ref. 8 was used to correct the results for all types of planform. In view of this result, the linear-theory estimates of $dC_L/d\eta_c$ and $dC_m/d\eta_c$ obtained for the inboard controls have been corrected for thickness in a similar manner. The linear-theory estimate of Ref. 7 assumes full lift carry-over at the outboard edges of the control (lift induced on the wing by the control pressure field

within the Mach cone from the control leading edge tip). There is some experimental evidence[10] to show that only part of this carry-over lift is realized in practice so that a second estimate of $dC_L/d\eta_c$ and $dC_m/d\eta_c$ has been obtained assuming the control tips to be unbounded by the wing. This solution (labelled 'no lift carry-over' in Figs. 28 and 29) is identical to that for an isolated rectangular wing[11] and it has been corrected for thickness effects in the manner of the solution with full lift carry-over. Both estimates have been corrected for sting-shroud interference using the linear-theory factors of Ref. 12.

An estimate has also been made of $dC_L/d\eta_c$ for the outboard controls. The linear-theory perturbation potential along the control trailing edge was calculated using Evvards method[13], and the overall lift obtained by numerical integration. Because of the amount of work involved only one solution (with full lift carry-over at the inboard edge of the control) was obtained, and this has been corrected for control-thickness effects as for the inboard control.

The derivatives $dC_l/d\xi_c$, $dC_L/d\eta_c$ and $dC_m/d\eta_c$ are plotted against Mach numbers in Figs. 27, 28 and 29 respectively. At $M = 1{\cdot}4$ the experimental results fall between the two estimates whereas at $M = 2{\cdot}2$ both estimates are too large. These results are in reasonable agreement with previous measurements of control effectiveness on a slender wing[14].

Measurements of the lift-effectiveness parameter $dC_{Lc}/d\eta_c$ (C_{Lc} is the lift coefficient based on control area) for rectangular and near rectangular controls have been collected from various sources, and are plotted in the form $1/A_c\, dC_{Lc}/d\eta_c$ against $A_c\sqrt{M^2-1}$ in Fig. 30. Figs. 30a and 30b show the results before and after correction for control thickness and body interference respectively. With the exception of the results from Ref. 15 there is fair correlation with a scatter of approximately ± 10 per cent on the mean curve. The corrections for control thickness and body interference improve the agreement with theory although the measured results still tend to be slightly low.

5.2.2. *Drag due to control deflection.* Theoretical expressions have been derived[14] for the effect of control deflection on the minimum drag coefficient and the lift coefficient at minimum drag. They are reproduced below:

$$\Delta C_{Dm} = a'_2\,\eta_c^2 + \left(\frac{a'_1+a'_2+a''_2}{a_1}\right)\eta_c\,(C_{Lm}-\Delta C_L) - \frac{\pi A}{K}\left[\frac{\eta_c\,(a'_1+a'_2+a''_2)}{2a_1}\right]^2 \tag{6}$$

$$\Delta C_{Lm} = (a'_2+a''_2)\,\eta_c - \frac{\pi A}{K}\left[\eta_c\,\frac{(a'_1+a'_2+a''_2)}{2a_1}\right] \tag{7}$$

where ΔC_{Dm} and ΔC_{Lm} are the increments in the minimum drag coefficient and in the lift coefficient at minimum drag respectively,

η_c is the control setting angle in radians, positive when the trailing edge is deflected downwards,

A the wing aspect ratio,

K the drag due to lift factor of the wing $\left(=\pi A\,\dfrac{dC_D}{dC_L^2}\right)$,

C_{Lm} is the lift coefficient at minimum drag with the controls undeflected,

ΔC_L is the lift on the wing when it is at zero incidence (measured relative to the undeflected controls).

$a_1 = (dC_L/d\alpha)$ wing per rad

$a'_1 = (dC_L/d\alpha)$ control per rad

$a'_2 = (dC_L/d\eta_c)$ control per rad

$a''_2 = (dC_L/d\eta_c)$ control carry-over lift per rad

} based on wing area.

Measured values of a_1, K, C_{Lm} and ΔC_L obtained with the controls undeflected have been used in the estimation of ΔC_{Dm} and ΔC_{Lm} together with linear theory values of a'_1 derived using Evvards' approximate method[16] and corrected for thickness effects in the manner of Ref. 8. Two calculations of ΔC_{Dm} and ΔC_{Lm} were performed, one using linear-theory values of a'_2 and a''_2 corrected for control thickness and body-interference effects (section 5.2.1) and another with the present measured values of a'_2 with a''_2 assumed to be zero.

Only fair agreement between theory and experiment is obtained using the theoretical values of a'_2 and a''_2 (Figs. 31 and 32), which is not surprising in view of the disparity shown in Fig. 28 between experimental values of $dC_L/d\eta_c$ and theory with full lift carry-over. Somewhat better agreement is obtained, especially for the outboard controls, when measured values of a'_2 are used. However, although it may be smaller than theory predicts, it is unlikely that a''_2 will be zero, so that part of the difference may be due to the use of incorrect values of a'_1 in the calculations.

5.2.3. *Control hinge moment.* The variation of C_H with α is slightly non-linear for both inboard and outboard controls (Figs. 33 and 34); however the variation with control setting angle η_c is linear (Fig. 35). Analysis of the hinge-moment derivative $dC_H/d\eta_c$ for rectangular controls on various wings[9] has demonstrated good experimental correlation and agreement with theory at supersonic speeds. The analysis of Ref. 9 was applied to the prediction of $dC_H/d\eta_c$ for the inboard controls on the present model. The linear-theory estimate for $dC_H/d\eta_c$ was first obtained assuming that the outboard edges of the control are free (the lift distribution along the control trailing edge becomes zero at the tip and there is no lift carry-over onto the adjacent wing). This estimate was then corrected for control thickness in the manner of Ref. 8 and for interference effects from the strong shroud using the linear theory factors of Ref. 12. Fig. 36a shows that good agreement is obtained between theory and experiment, the predicted values of $dC_H/d\eta$ being approximately $6\frac{1}{2}$ per cent too high.

Although estimated values of $dC_L/d\eta_c$ for the outboard control were obtained using Evvards' method[13], the method was considered to be too laborious for the calculation of $dC_H/d\eta$. Czarnecki and Lord[17] have shown that for controls with horn balances a linear relationship exists between $dC_H/d\eta$ and the ratio of the horn area (defined as that area ahead of the hinge line) to control total area. Using the method of Ref. 9 an estimate of $dC_H/d\eta$ was calculated for a rectangular control having the same area and span as the outboard control with its hinge line at the leading edge. The experimental results of Ref. 17 were used to obtain the horn area ratio for complete balance (39 per cent). This ratio was assumed to be constant for all Mach numbers and was used to obtain a factor which was then applied to the rectangular control value of $dC_H/d\eta$. Fig. 36b shows both the theoretical curve for the rectangular control and the factored curve, but the measured values agree with the latter only at $M = 2{\cdot}2$, falling between the two theoretical curves at lower Mach numbers. It would appear that a more thorough theoretical treatment is necessary in order to predict accurately the hinge-moment characteristics of controls with horn balances.

Evvards' approximate method[16] was used to calculate linear-theory values of $dC_H/d\alpha$ for both inboard and outboard controls, the appropriate factor from Ref. 8 being applied to correct these for control thickness effects. For the inboard controls (Fig. 36c) the predicted values of $dC_H/d\alpha$ agree well with experiments; however the measured values of $dC_H/d\alpha$ for the outboard controls are in general much larger than theory and in addition they exhibit a large variation with incidence, possibly due to leading-edge flow-separation effects (Fig. 36d).

5.3. *Lateral Stability and Fin Effectiveness.*

5.3.1. *Basic wing body.* The main feature of the lateral-stability measurements at $M = 0{\cdot}275$ is the non-linear variation of C_Y with β (Fig. 37). The unusual behaviour of C_Y at $\alpha = 11{\cdot}66°$ could possibly be due to some asymmetric flow over the model. The same asymmetry is present with the fin on (section 5.3.2). At supersonic speeds non-linearities are present at high incidence (Fig. 38). The variation of C_n and C_l with β at all speeds requires no comment (Figs. 37, 39, and 40).

The derivatives y_v, n_v and l_v defined as $(dC_Y/d\beta)_{\beta=0}$, $(dC_n/d\beta)_{\beta=0}$ and $(dC_l/d\beta)_{\beta=0}$ respectively, where β is in radians, are plotted in Fig. 41. At $M = 0{\cdot}275$, y_v changes from negative to positive with increasing α. This type of variation has been observed before[14], and is thought to be due to flow separation effects (wing vortices becoming asymmetric under conditions of yaw). The slender-body theory estimate[18] of y_v at zero incidence is much too low (Fig. 41a), so that although the absence of a sting shroud full scale would probably result in a smaller y_v, it is not possible to calculate the size of the reduction. The value of n_v for stability axes changes sign with increasing incidence (Fig. 41a), but this variation is due solely to the resolved component of l_v referred to body axes, n_v in body axes remaining constant. In general the slope of the l_v with α curve is predicted by slender-body theory[18] (flat-plate model), although as might be expected from the flat-plate assumptions this estimate does not give the correct value of l_v at $\alpha = 0°$.

In general, at supersonic speeds both y_v and n_v increase slightly with increasing Mach number and there is no significant variation with incidence (Fig. 41b). The slender body estimate[18] of y_v is again much too low. $dl_v/d\alpha$ decreases with increasing Mach number and there are also slight variations with incidence. Linear theory estimates[19] of l_v referred to body axes at supersonic speeds have been obtained for the present wing. For these estimates the effect of camber, the presence of the body and the cropped wing tips were all ignored. The measured values of $dl_v/d\alpha$ at low incidence, where the wing flow is attached, are in fair agreement with theory at $M = 1{\cdot}4$ and $1{\cdot}8$ (Fig. 42) but the measured values at high incidence are all much less than predicted. At $M = 2{\cdot}2$, the comparison between theory and experiment is poor at all incidences. As at subsonic speeds (Fig. 41) the correct value of l_v at zero incidence was not predicted by the theory due to the flat-plate assumptions.

5.3.2. *Effect of fin and nacelles.* The plots of C_Y, C_n and C_l against β are shown in Figs. 43 to 46 for the configuration with fin and in Figs. 47 to 49 for the configuration with nacelles. The majority of these results are straightforward, however, although the variation of C_Y with β at $M = 0{\cdot}275$ is more linear for the configuration with fin (Fig. 43), than for the basic wing-body (Fig. 37), the large positive value of C_Y at zero β at $\alpha = 11{\cdot}66°$ is still present.

The addition of the fin makes the wing laterally stable with the present cg position at all the Mach numbers tested (Figs. 50 and 52) and although $-l_v$ is increased at supersonic speeds (Fig. 53) there is a substantial reduction at $M = 0{\cdot}275$ at high incidence (Fig. 50). The nacelles increase $-y_v$ at all incidences (Fig. 51), but the effect on n_v is much smaller (Fig. 52) due to the proximity of the nacelle centre of pressure to the moment reference centre.

The prediction of the lift-curve slope of the isolated fin presents some problems because of its planform shape. Linear theory estimates of $dC_L/d\alpha$ for a 'double-delta' fin, having the same root chord and leading-edge sweepback angles as the present fin but without the cropped tip, were obtained over a limited Mach number range ($1{\cdot}52$ to $1{\cdot}78$) from the charts of Ref. 20. These values were then compared with others obtained by taking the lift-curve slopes of the rear delta (leading-edge sweepback 58° 33′) and adjusting these to the larger reference area of the 'double-delta'. In other words, the lift on that part of a 'double-delta' forward of the crank in the leading edge is assumed to be independent of the leading-edge sweepback forward of the crank. For slender shapes this is a reasonable assumption and in fact follows from slender body theory. Providing that the forward part of the double delta is small compared with the rest of the wing (as in the present case), then the lift on the rear of the wing will not be significantly affected by the shape of the forward part. Over this limited range of Mach number it was found that the two estimates of lift curve slope agreed to within 3 per cent. It was therefore decided that, for the present fin which has a cropped tip, only the second method would be used, that is, the lift-curve slope of a cropped delta with 58° 33′ leading-edge sweepback would be adjusted to the reference area of the cropped 'double-delta', and that this method would be used for all Mach numbers.

Estimates of $\Delta y_{v_{\text{Fin}}}$, the increment in y_v due to the fin, have been obtained using the above values of lift-curve slope and making allowance for interference between fin and sting shroud with the methods of Ref. 21. At $M = 0{\cdot}275$ this estimate is much too large (50 per cent) (Fig. 54), and much better agreement is obtained between experiment and a predicted value based on fin lift alone, i.e. a fin added to a reflection plane. At supersonic speeds the estimates based on the method of Ref. 21 are again much too large, in this case they are beyond the range of each graph and have been omitted from Fig. 55. The empirical

wing body interference factors from standard methods are somewhat smaller than the slender body factors of Ref. 21 but even these give estimates which are too large (Fig. 55). The fin lift alone estimates are slightly less than the measured values as at subsonic speeds. Because of this difficulty in accurately predicting the fin effect on y_v no attempt has been made to predict the fin effect on either n_v or l_v (Figs. 56 and 57 respectively).

6. *Conclusions.*

Although the agreement between measured and predicted[6] values of the lift and pitching-moment increments due to the fin was only fair, it was thought that this was because the theory was not fully representative of the present model.

Fair correlation was obtained between the measured lift effectiveness of the inboard controls and results from other sources including both part span and full span rectangular trailing edge controls. After suitable corrections for control thickness and control-body interference effects had been applied the experimental results were only slightly lower than the linear-theory estimate for a full-span rectangular control for $A_c\sqrt{M^2-1} > 2$.

It was possible to estimate the drag due to the controls with fair accuracy providing that accurate values of the control lift effectiveness were used in the calculations.

Measured values of the hinge-moment derivatives $dC_H/d\alpha$ and $dC_H/d\eta$ for the inboard controls were in good agreement with theory, but for the outboard controls the agreement varied from fair to poor.

Slender-body theory was inadequate for predicting y_v for the basic wing-body combination both at subsonic and supersonic speeds. Measured values of $dl_v/d\alpha$ were in good agreement at subsonic speeds with slender-body theory estimates and at low supersonic speeds and low incidences with linear-theory estimates.

It was not possible to estimate the contribution of the fin to y_v with any accuracy.

LIST OF SYMBOLS

A	Aspect ratio
a_1	$(dC_L/d\alpha)$ wing
a_1'	$(dC_L/d\alpha)$ control
a_2'	$(dC_L/d\eta_c)$ control
a_2''	$(dC_L/d\eta_c)$ control carry-over lift
b	Wing span
c	Chord
c_0	Root chord
$\bar{c}$	Standard mean chord
$\bar{\bar{c}}$	Aerodynamic mean chord
C_L	Lift coefficient, lift/qS (positive upwards)
C_{Lc}	Control lift coefficient, based on control area
C_m	Pitching-moment coefficient, pitching moment/$qS\bar{c}$ (positive nose upwards)
C_D	Drag coefficient, drag/qS (positive backwards)
C_x	Axial-force coefficient, axial force/qS (positive backwards along sting axis)
C_Y	Side-force coefficient, side force/qS (positive to starboard)
C_n	Yawing-moment coefficient, yawing moment/qSb (positive nose to starboard)
C_l	Rolling-moment coefficient, rolling moment/qSb (positive starboard wing downwards)
C_H	Hinge-moment coefficient, hinge moment/qS_cC_c (positive trailing edge downwards)
K	Drag due lift factor of wing $= \pi A\, dC_D/dC_L^2$
K_ϕ	Control-thickness factor for lift and hinge moment at supersonic speeds (*see* Ref. 9)
$k_{w(B)}$	Wing-body or control-body interference factors (*see* Ref. 12)
$k_{B(w)}$	
L	Length of model with short shroud (nose to wing trailing edge)
l	Length of nacelles
l_v	$(dC_l/d\beta)_{\beta=0}$ with β in radians
M	Mach number
n_v	$(dC_n/d\beta)_{\beta=0}$ with β in radians
q	Free stream kinetic pressure
R	Reynolds number
S	Wing reference area
$S(x)$	Cross section area
y_v	$(dC_Y/d\beta)_{\beta=0}$ with β in radians

per radian based on wing area

of gross wing (for numerical values *see* Table 1)

x	right hand system of axes	x positive backwards
y		y positive to starboard
z		z positive downwards
α	Incidence angle	
β	Sideslip angle	
θ	Total incidence angle	
ϕ	Roll angle measured from the trailing edge horizontal	
η_c	Control setting angle for controls deflected as elevators (positive trailing edge down)	
ξ_c	Control setting angle for controls deflected as ailerons (positive trailing edge up for port control, trailing edge down for starboard control)	

Suffices

c	Refers to control
m	Refers to conditions at minimum drag

REFERENCES

No.	Author(s)	Title, etc.
1	B. Furness	Summary of design philosophy and zero-lift drag characteristics of the 500 series wind tunnel models. Bristol Aircraft Ltd., Aero Report 198/58 (1961).
2	C. R. Taylor	Measurements at Mach number up to 2·8 of the longitudinal characteristics of one plane and three cambered slender ogee wings. A.R.C. R. & M. 3328 (1961).
3	D. Isaacs	Unpublished Mintech work.
4	T. A. Cook	Unpublished data from R.A.E. tests.
5	S. B. Berndt	Wind tunnel interference due to lift for delta wings of small aspect ratio. KTH–Aero T.N.19 Sweden (1952).
6	L. B. Jones	The effects on wing lift and pitching moment due to the fin of an aircraft flying at supersonic speeds. English Electric Aviation Ltd., Aero Research Report No. 1 (1961).
7	W. A. Tucker and R. L. Nelson	Characteristics of thin triangular wings with constant-chord partial span control surfaces at supersonic speeds. NACA T.N. 1660 (1948).
8	W. A. Tucker and R. L. Nelson	Theoretical characteristics in supersonic flow of constant-chord partial span control surfaces on rectangular wings having finite thickness. NACA T.N. 1708 (1948).
9	D. Isaacs	Analysis of hinge moment data for rectangular and near rectangular trailing edge controls at supersonic and transonic speeds. A.R.C. C.P. 874 (1965).
10	D. R. Lord and K. R. Czarnecki	Pressure distributions and aerodynamic loadings for several flap type trailing-edge controls on a trapezoidal wing at Mach numbers of 1·61 and 2·01. NACA R. & M. L55J03 (TIL 5013) (1956).
11	P. A. Lagerstrom and M. E. Graham	Low aspect ratio rectangular wings in supersonic flow. Douglas Aircraft Co. Report SM–13110 (1947).
12	W. C. Pitts, J. N. Nielsen and G. E. Kaattari	Lift and center of pressure of wing-body-tail combinations at subsonic, transonic and supersonic speeds. NACA Report 1307 (1957).
13	J. C. Evvard	Distribution of wave drag and lift in the vicinity of wing tips at supersonic speeds. NACA T.N. 1382 (1947).

REFERENCES—*continued*

No.	*Author(s)*	*Title, etc.*
14	D. Isaacs	Measurements at subsonic and supersonic speeds of the longitudinal and lateral stability of a slender cambered ogee wing including the effects of a fin, canopy nose and trailing edge controls. A.R.C. R. & M. 3390 (1963).
15	L. D. Guy	Hinge moment and effectiveness of an unswept constant-chord control and an overhang-balanced, swept hinge-line control on an 80° swept-pointed wing at Mach numbers from 0·75 to 1·96. NACA RM L56F11 (TIL 5211) (1956).
16	J. C. Evvard	The effects of yawing thin pointed wings at supersonic speeds. NACA T.N. 1429 (1947).
17	K. R. Czarnecki and D. R. Lord	Hinge-moment characteristics for several tip controls on a 60° sweptback delta wing at Mach number 1·61. NACA RM L52K28 (TIB 3598) (1953).
18	A. H. Sacks	Aerodynamic forces, moments, and stability derivatives for slender bodies of general cross section. NACA T.N. 3283 (1954).
19	H. S. Ribner and F. S. Malvestuto	Stability derivatives of triangular wings at supersonic speeds. NACA Report 908 (1948).
20	H. Behrbohm	The method of upwash-cancellation in linearised supersonic wing theory as applied to the double-delta wing with subsonic leading edges. I. Total lift and pitching moment in symmetrical flow conditions. SAAB T.N. 18 (1953).
21	F. K. Goodwin and G. E. Kaattari	Estimation of directional stability derivatives at small angles and subsonic and supersonic speeds. NASA Memo 12–2–58A (TIL 6338) (1958).
22.	L. D. Gay	Hinge-moment and effectiveness characteristics of an aspect-ratio 8·2 flap-type control on a 60° delta wing at Mach numbers from 0·72 to 1·96. NACA RM L56J17 (TIL 5382) (1957).
23.	L. D. Guy	Effects of overhang balance on the hinge-moment and effectiveness characteristics of an unswept trailing edge control on a 60° delta wing at transonic and supersonic speeds. NACA RM L54G12a (TIB 4390) (1954).
24	J. W. Boyd	Aerodynamic characteristics of two 25 per cent area trailing-edge flaps on an aspect ratio 2 triangular wing at subsonic and supersonic speeds. NACA RM A52 DOIC (TIB 3260) (1952).

No.	*Author(s)*	*Title, etc.*
25	D. R. Lord and K. R. Czarnecki	Aerodynamic characteristics of several flap-type trailing-edge controls on a trapezoidal wing at Mach numbers of 1·61 and 2·01. NACA RM L54D19 (TIB 4255) (1954).

TABLE 1

Principal Dimensions of Model

Overall length of model, L	56·855 in
Wing span, b	28·093 in
Wing root chord (gross wing) C_0	36·789 in
Wing standard mean chord (gross wing), $\bar{c}$	19·390 in
Wing aerodynamic mean chord (gross wing), $\bar{c}$	24·610 in
Wing reference area (gross wing), S	544·7 sq in
Distance of moment reference centre from wing trailing edge	12·305 in
Incidence of wing-root chord relative to OH datum	3° 36′
Incidence of sting-balance axis relative to OH datum	4° 20′
Incidence of wing trailing-edge plane relative to OH datum	0° 42′
Wing leading-edge sweepback	68°
Inboard control plan area	11·484 sq in
Inboard control chord	3·350 in
Inboard control mean included trailing-edge angle	7·30°
Outboard control plan area	15·899 sq in
Outboard control reference chord	3·150 in
Outboard control mean included trailing-edge angle	6·00°
Fin plan area	52·296 sq in

TABLE 2

Setting Angles of Unloaded Controls

Nominal settings	0°	+3°	−3°	+6°	−6°
Port outboard	0°	+2·90°	−3·23°	+6·23°	−6·57°
Port inboard	0°		−3·05°		−6·53°
Starboard outboard	0°	+3·32°	−3·20°	+6·42°	−6·38°
Starboard inboard	0°		−2·58°		−6·13°

Positive angles are for trailing edge deflected downwards.

TABLE 3

Test Details

Run No.	Sting shroud length	Fin	Nacelles	Inboard controls (positive trailing edge down)	Outboard controls (positive trailing edge down)	Type of measurement			Test Mach numbers
						Longitudinal stability drag. control effectiveness and hinge moments	Lateral stability	Pressure measurements for determining nacelle flow corrections to axial flow	
1	Short	Off	Off	0°	0°	No	No	Yes	1·8, 2·2
2	Short	Off	Off	0°	0°	No	No	Yes	1·4
3	Short	Off	On	0°	0°	No	No	Yes	1·8, 2·2
4	Short	Off	Off	−3°	0°	Yes	No	No	1·4, 1·8, 2·2
5	Short	Off	Off	−6°	0°	Yes	No	No	1·4, 1·8
6	Short	Off	Off	−6°	0°	Yes	No	No	1·4, 1·8, 2·2
7	Short	Off	Off	0°	0°	Yes	Yes	No	0·275, 1·4, 1·8, 2·2
8	Short	Off	On	0°	0°	Yes	Yes	No	1·8, 2·2
9	Short	Off	Off	0°	−3°	Yes	No	No	1·4, 1·8, 2.2
10	Short	Off	Off	0°	−6°	Yes	No	No	1·4, 1·8, 2·2
11	Short	Off	Off	0°	Port +3° Stbd −3°	Yes	No	No	1·4, 1·8, 2·2
12	Short	Off	Off	0°	Port +6° Stbd −6°	Yes	No	No	1·4, 1·8, 2·2
13	Long	On	Off	0°	0°	Yes except for hinge moments	Yes	No	0·275, 1·4, 1·8, 2·2

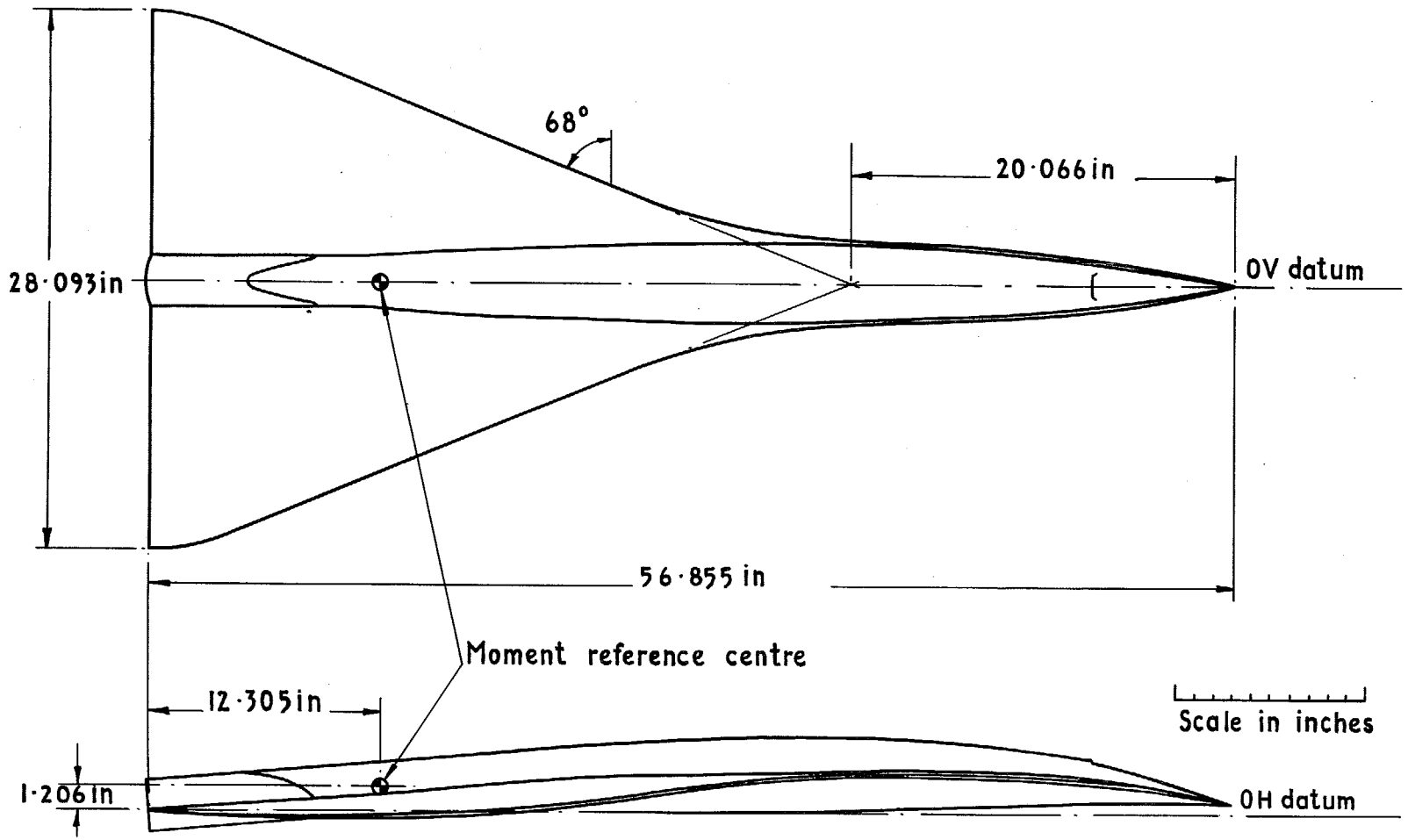

FIG. 1. Basic wing-body shape.

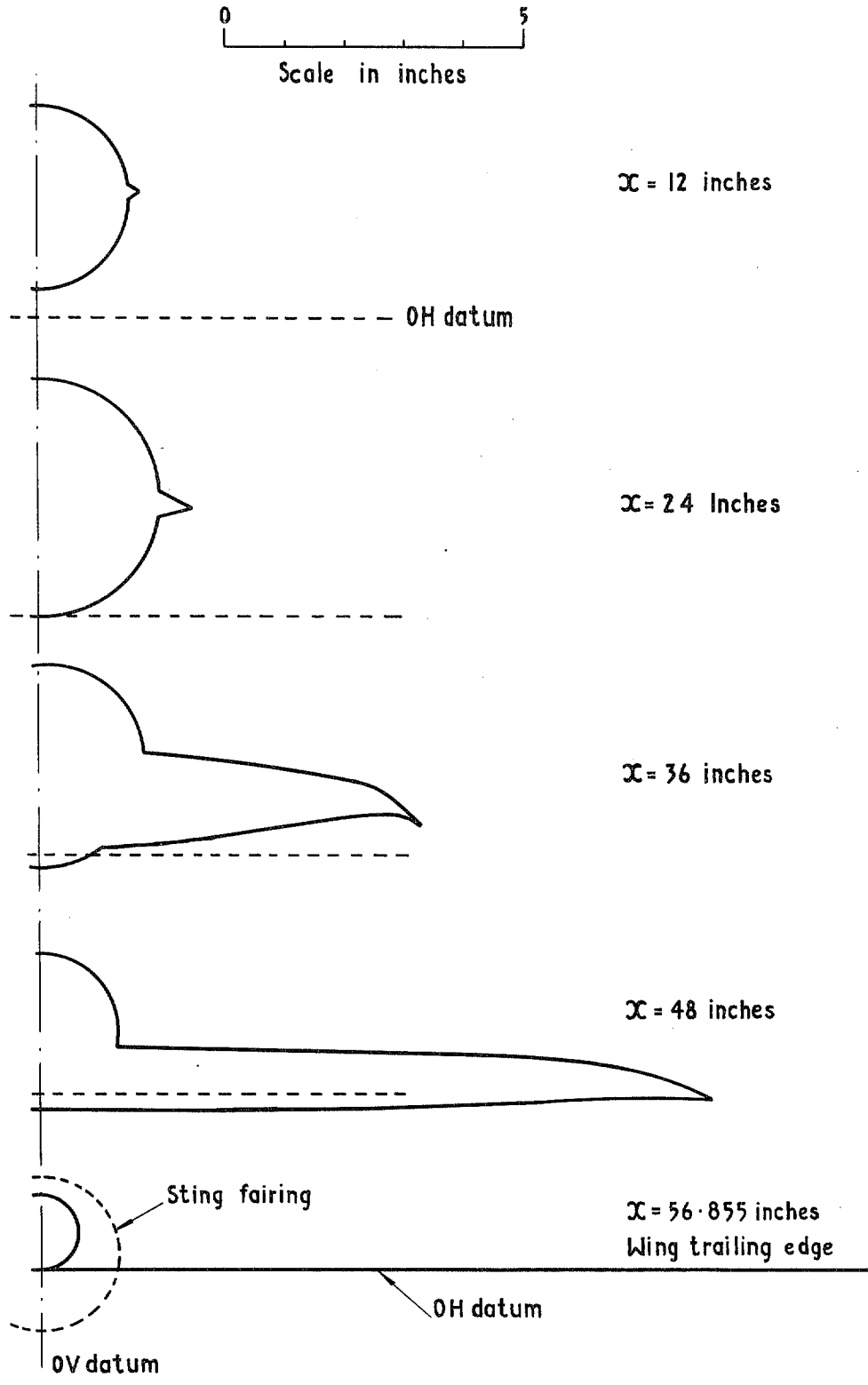

FIG. 2. Details of wing-body cross-section.

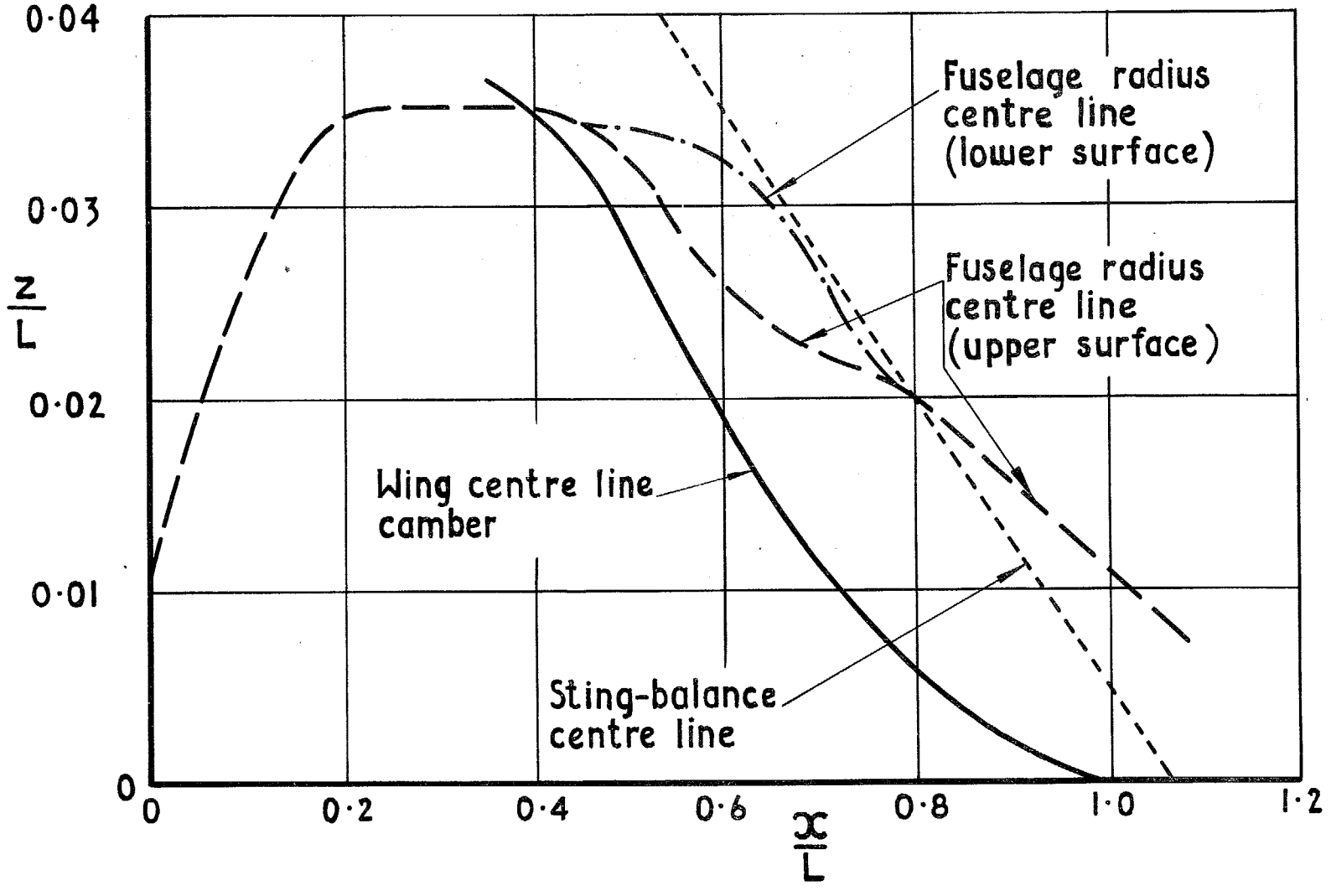

FIG. 3. Chordwise camber details (relative to O.H. datum).

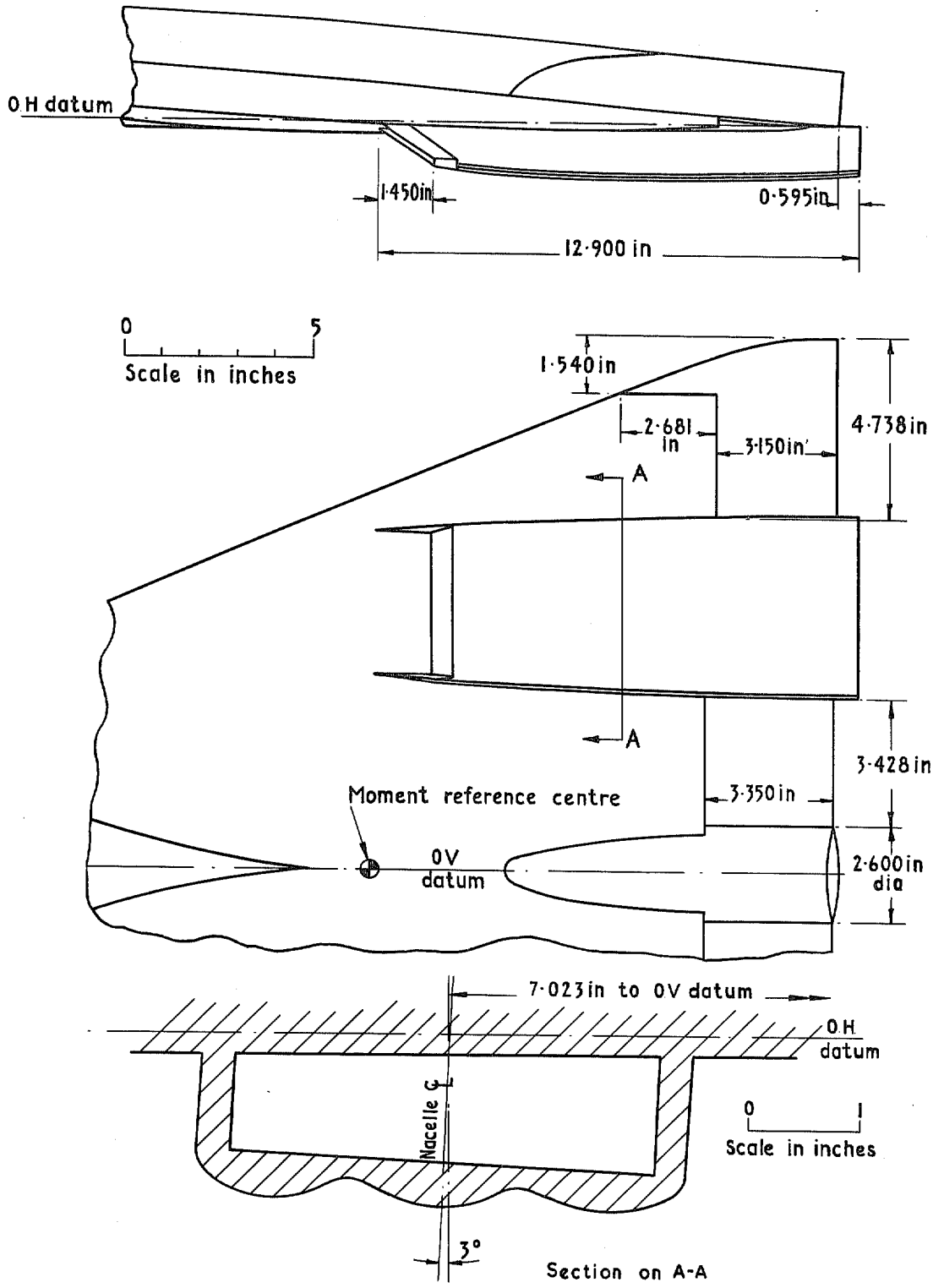

FIG. 4. Details of nacelles and controls.

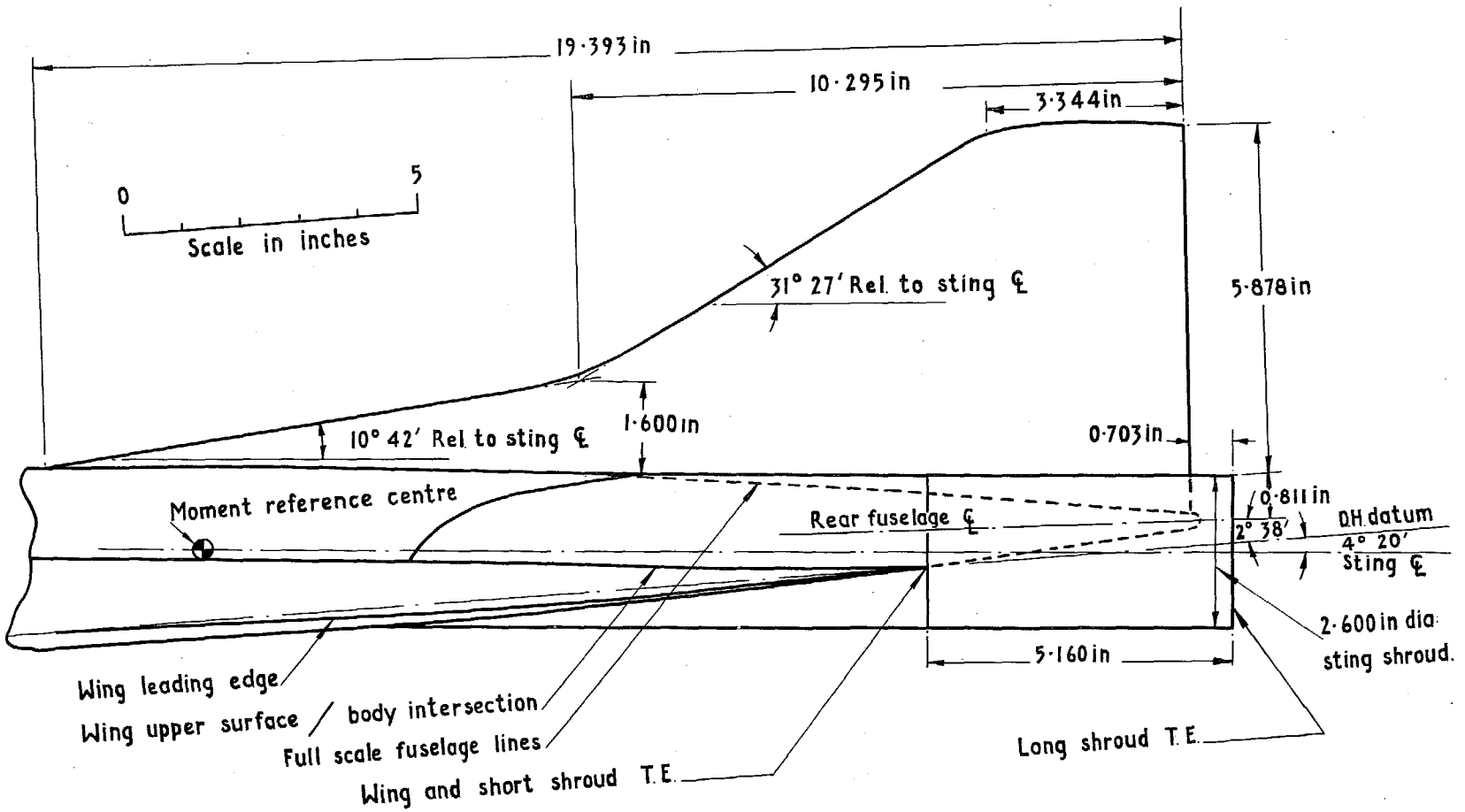

FIG. 5. Details of fin and rear fuselage distortion.

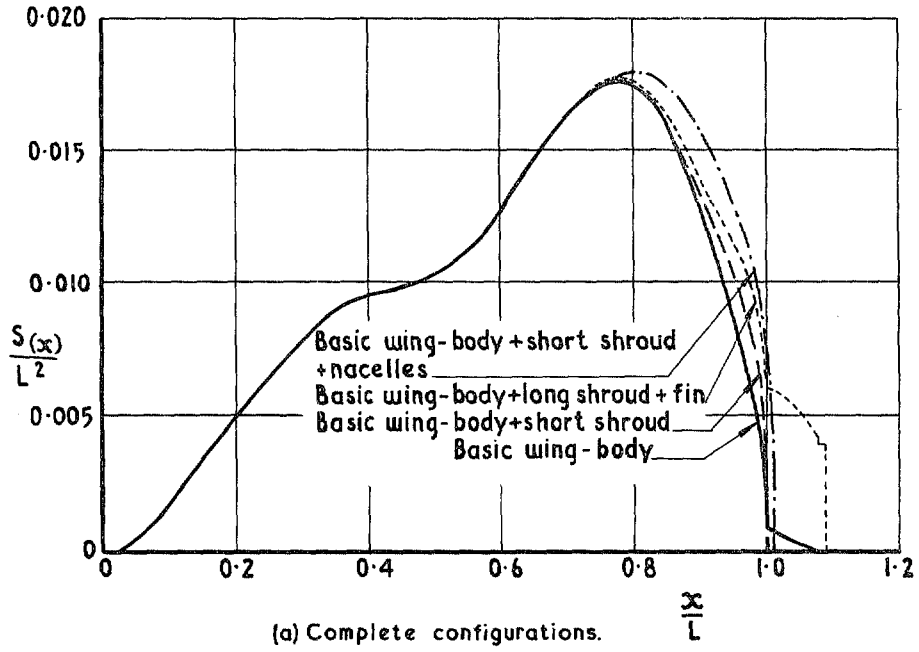

FIG. 6. Cross-section area distribution.

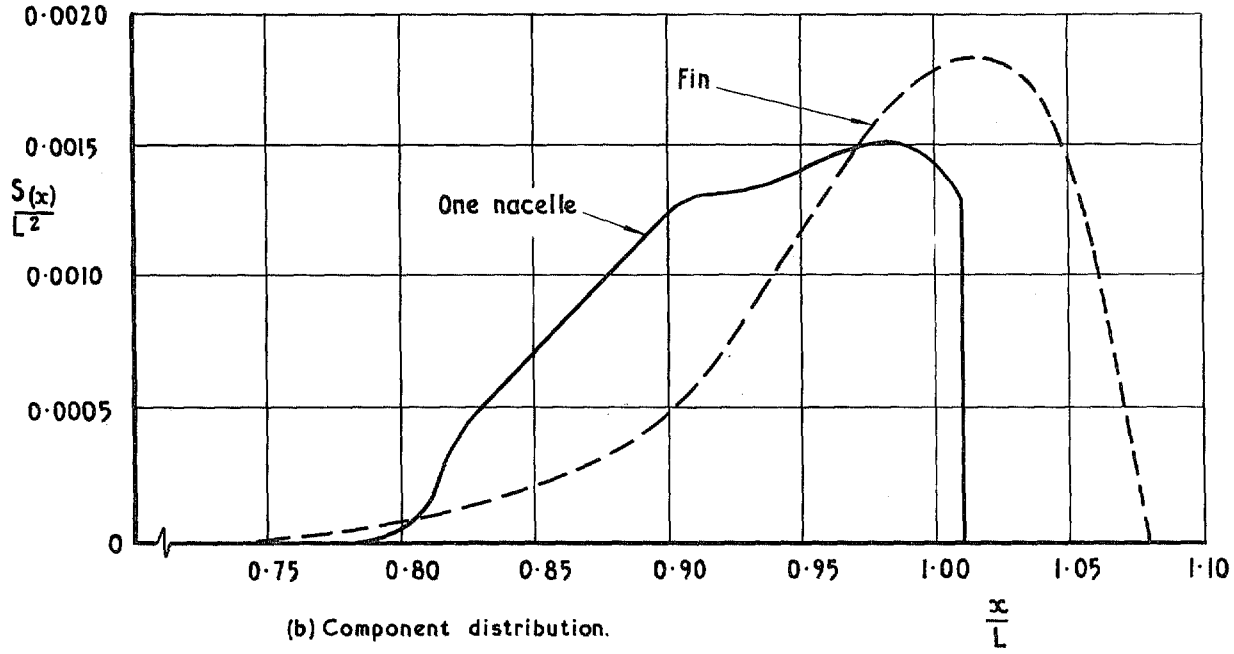

FIG. 6 (*contd.*)

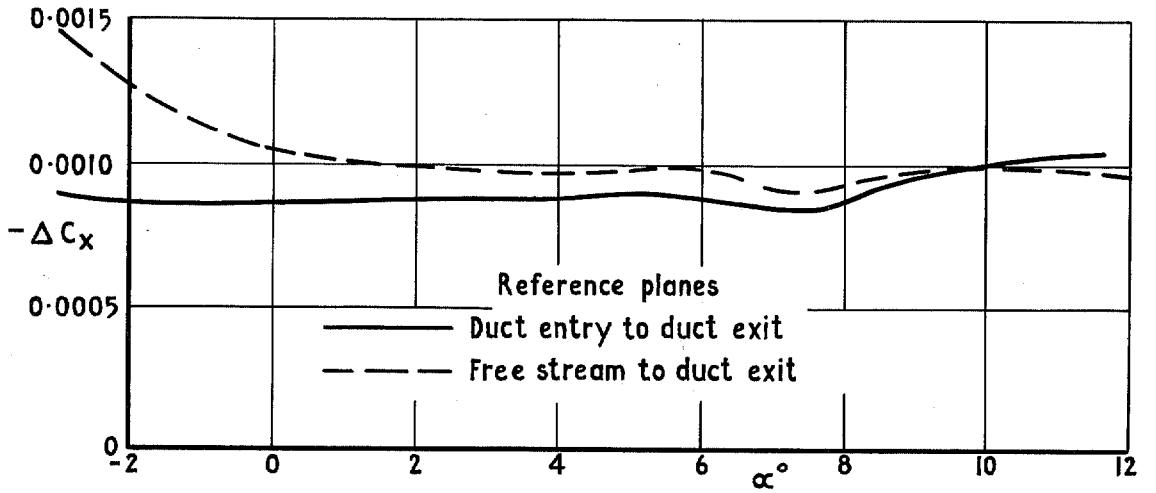

(a) M = 1·8

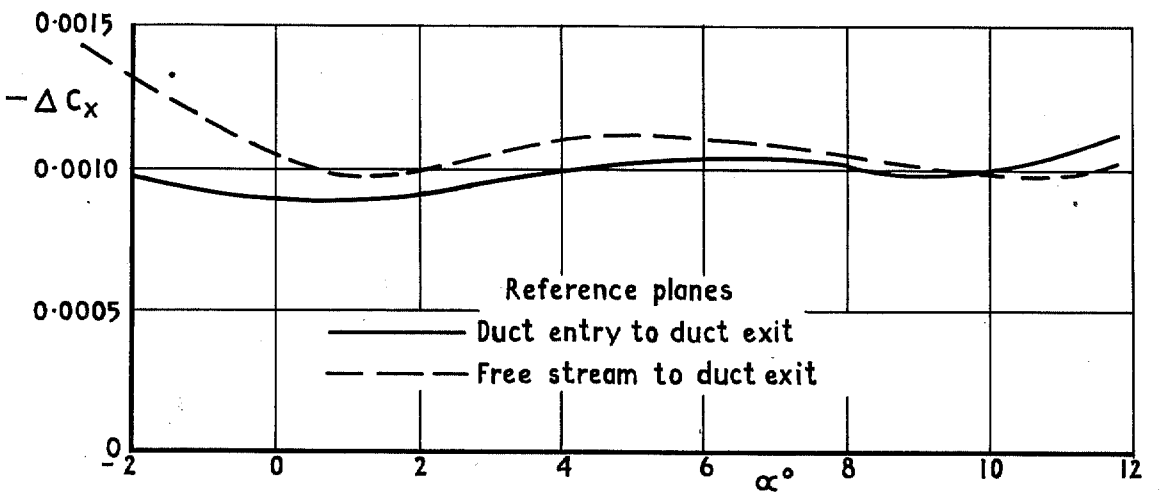

(b) M = 2·2

FIG. 7. Nacelle internal flow correction to axial force (one nacelle).

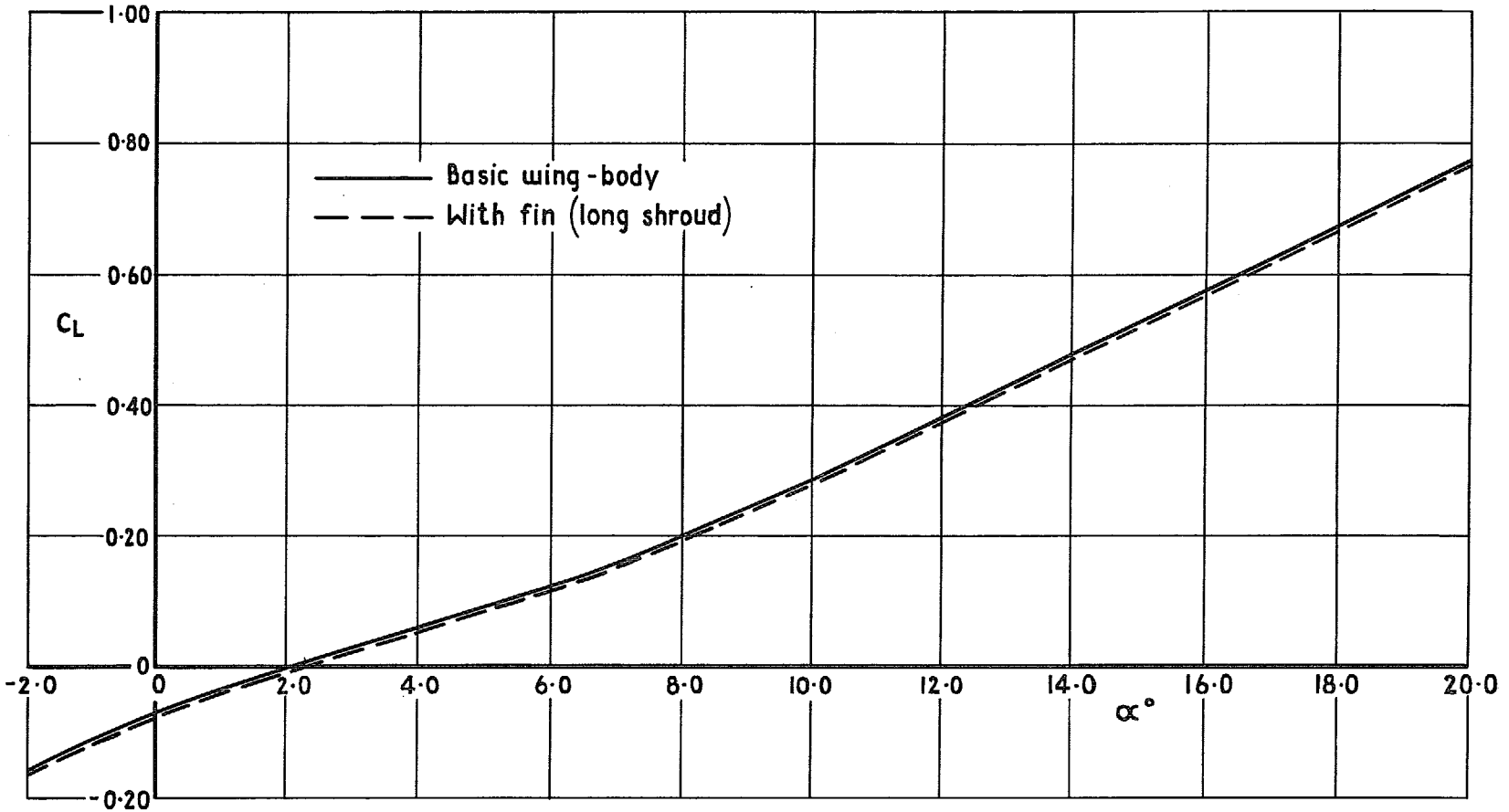

FIG. 8. Effect of fin on lift at subsonic speeds ($M = 0{\cdot}275$).

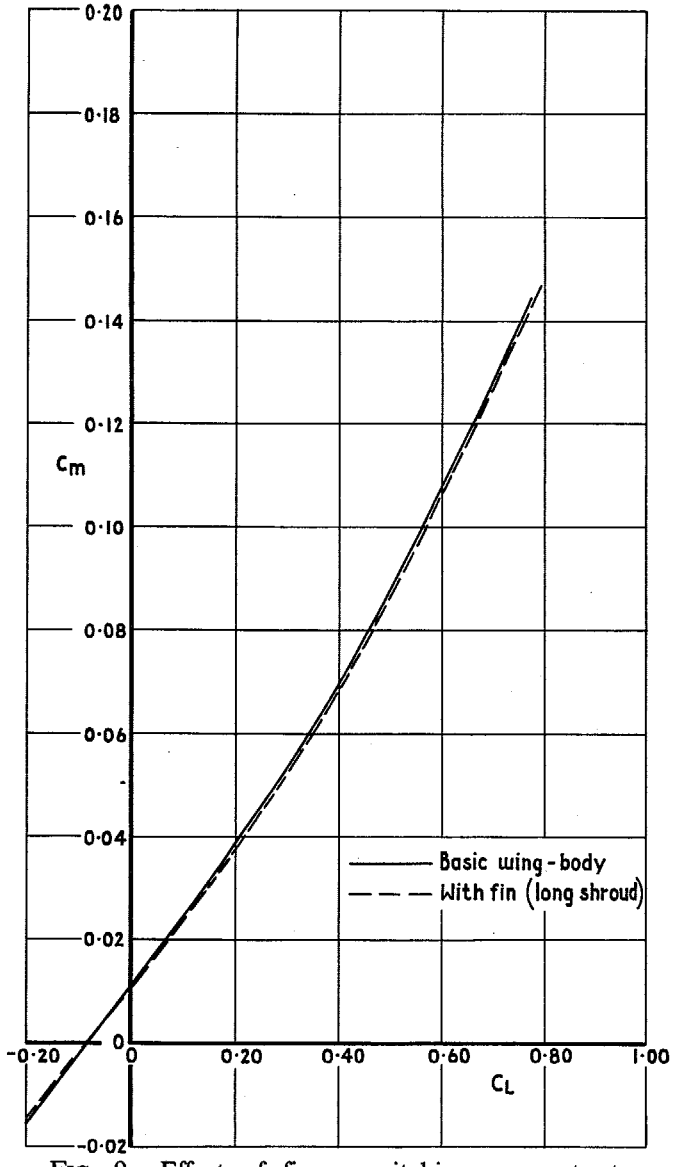

FIG. 9. Effect of fin on pitching moment at subsonic speeds ($M = 0{\cdot}275$).

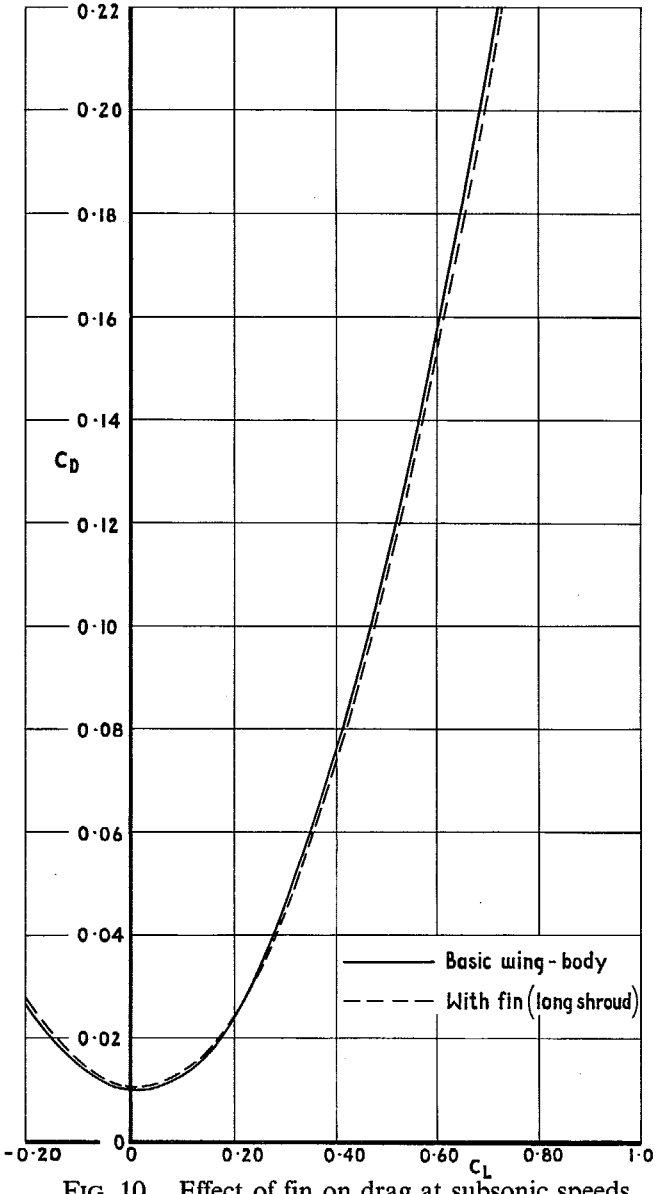

FIG. 10. Effect of fin on drag at subsonic speeds ($M = 0{\cdot}275$).

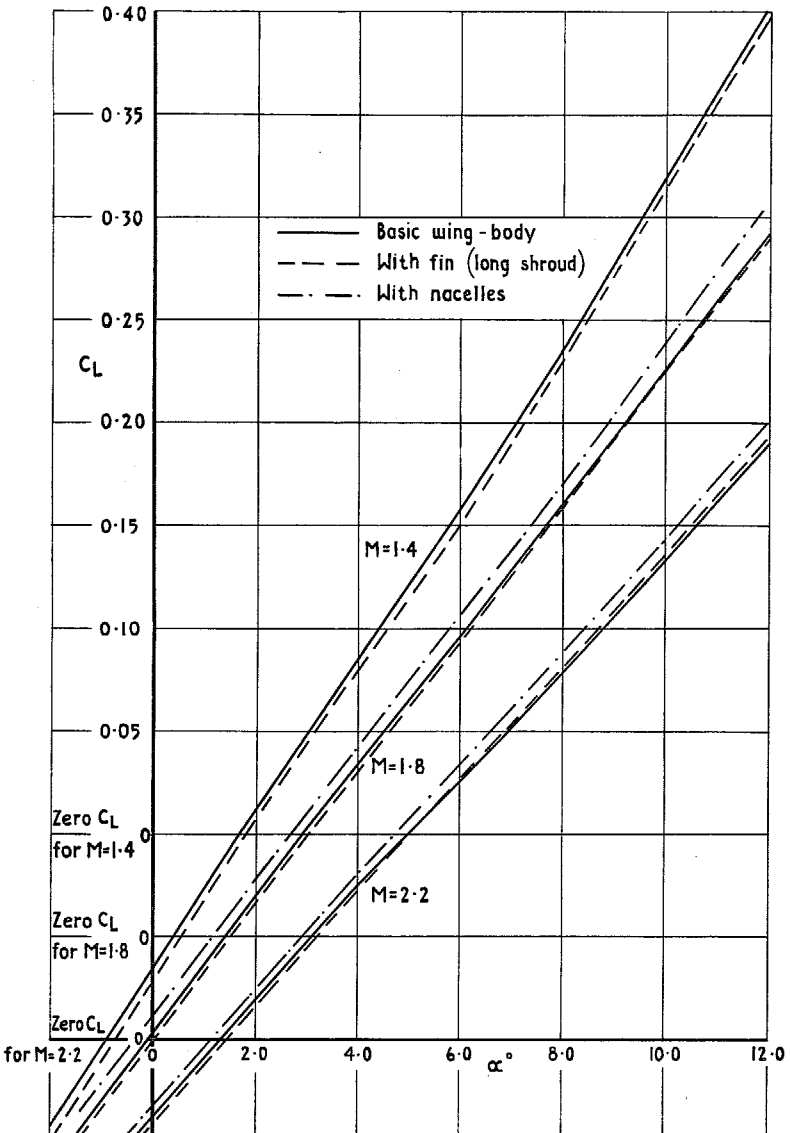

FIG. 11. Effect of fin and nacelles on lift at supersonic speeds.

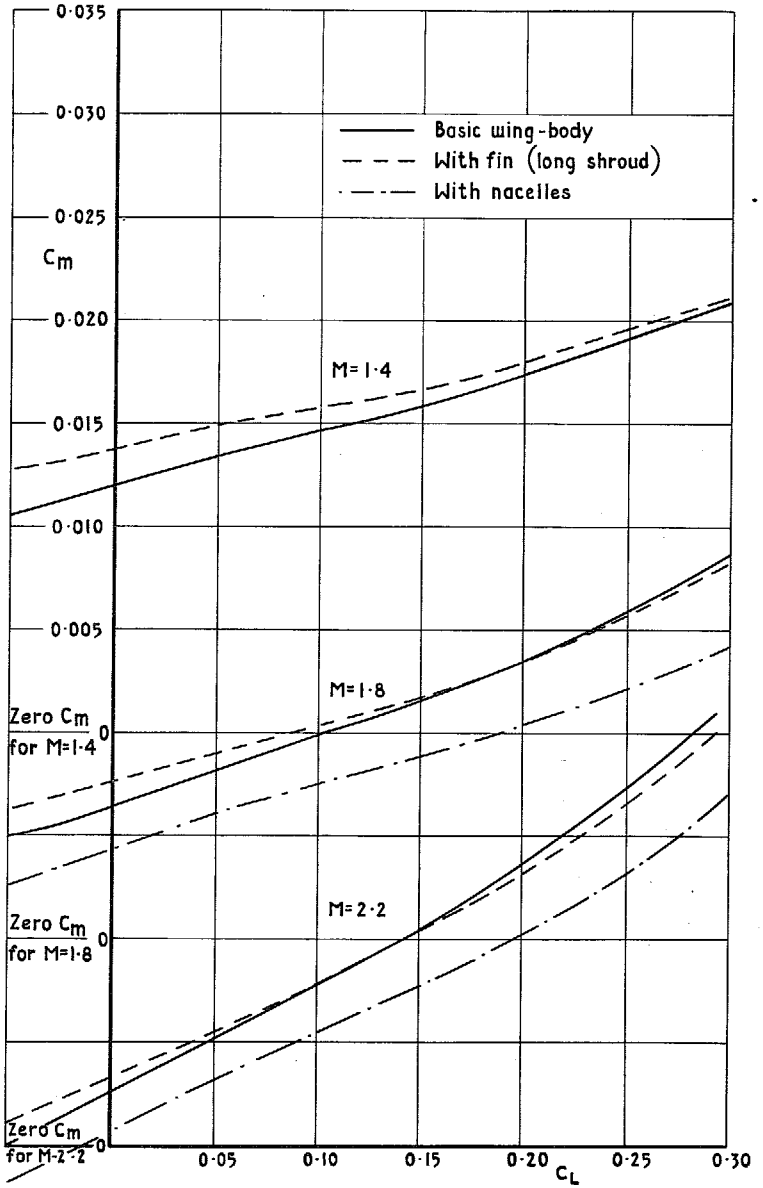

FIG. 12. Effect of fin and nacelles on pitching moment at supersonic speeds.

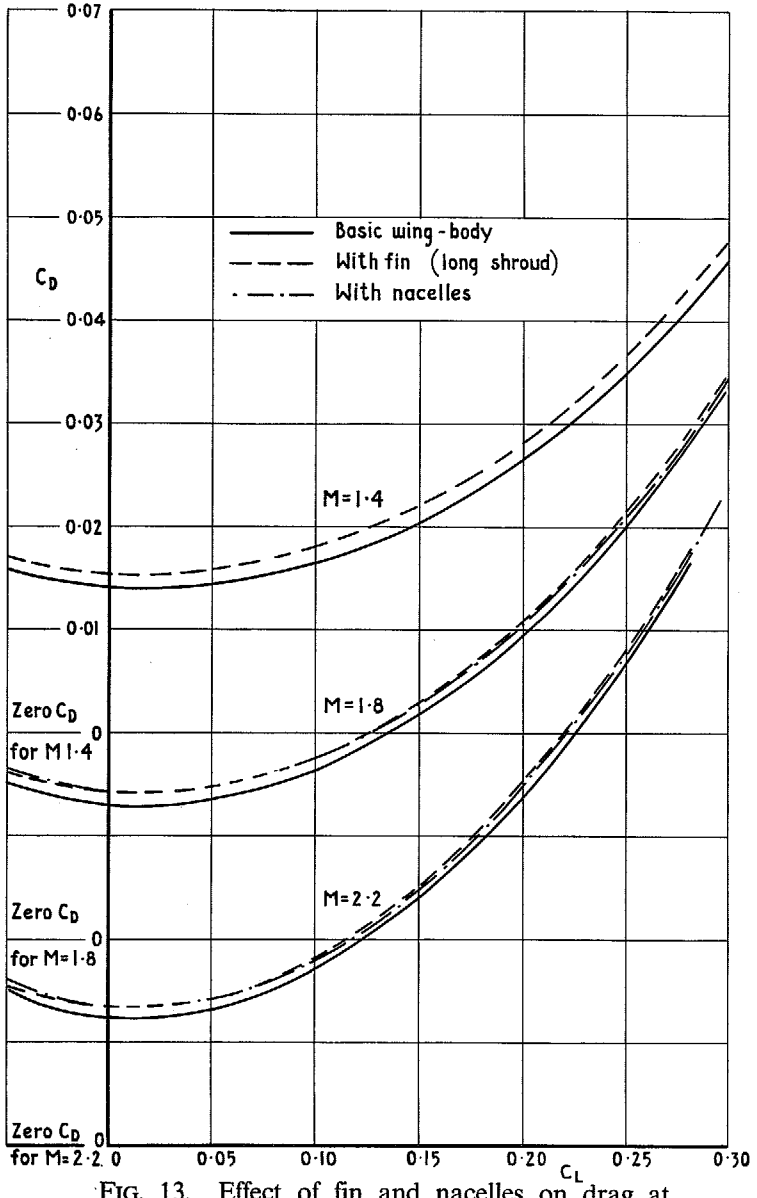

FIG. 13. Effect of fin and nacelles on drag at supersonic speeds.

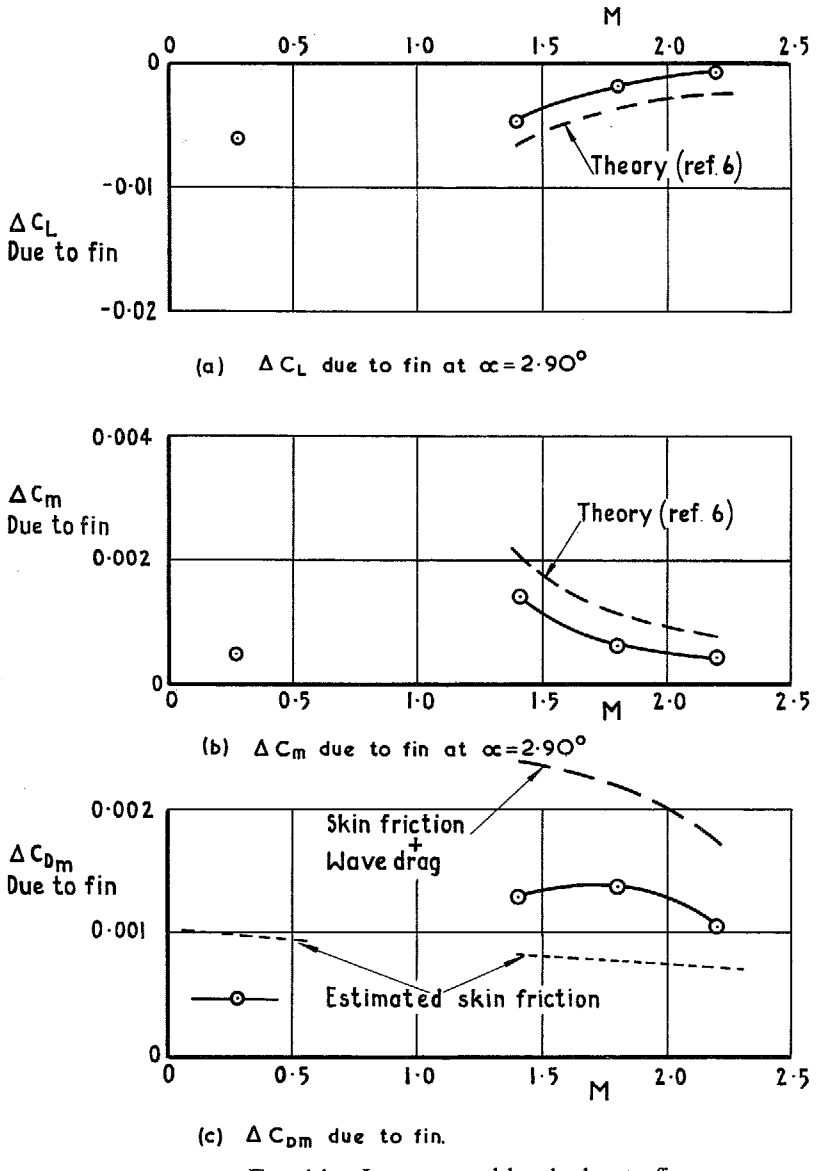

FIG. 14. Incremental loads due to fin.

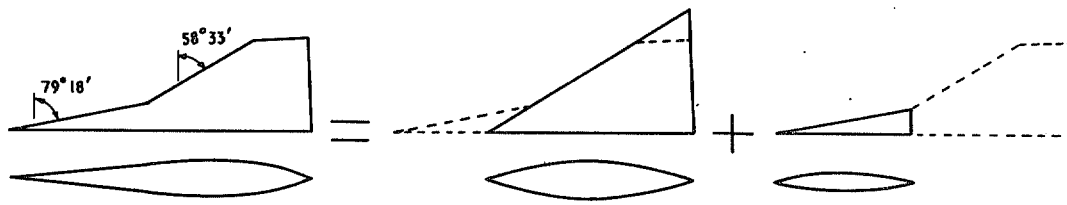

FIG. 15. Model used for theoretical estimates of lift and pitching moment due to fin.

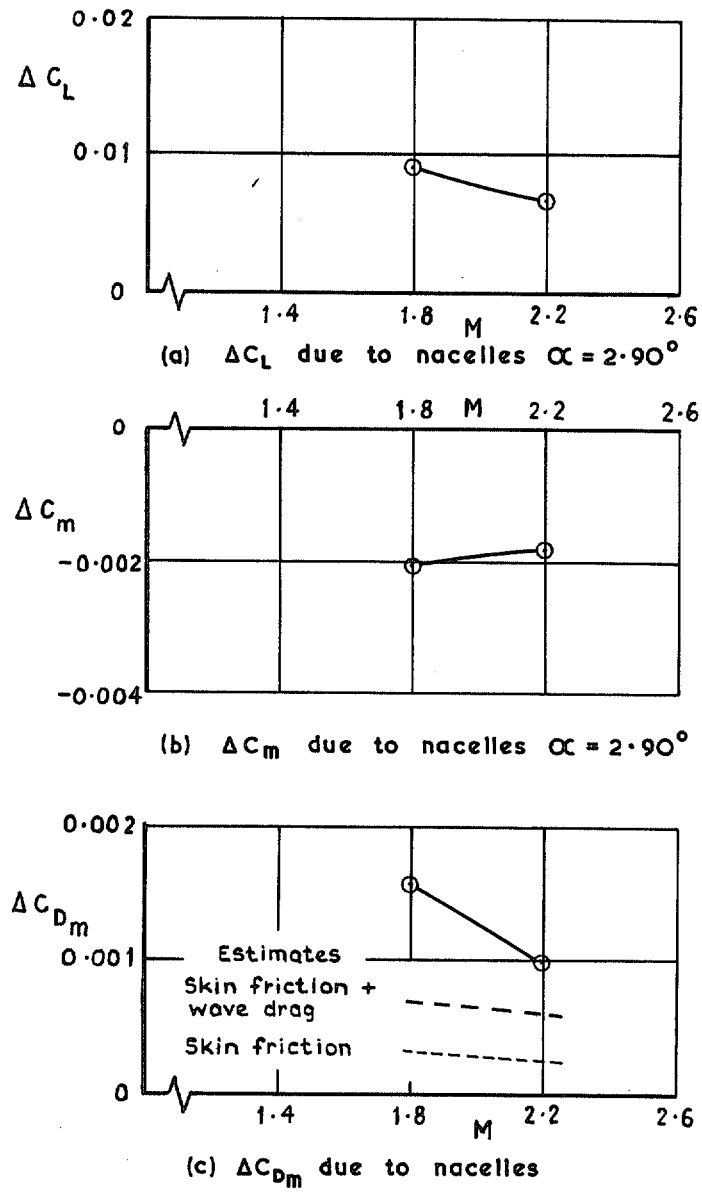

FIG. 16. Incremental loads due to nacelles.

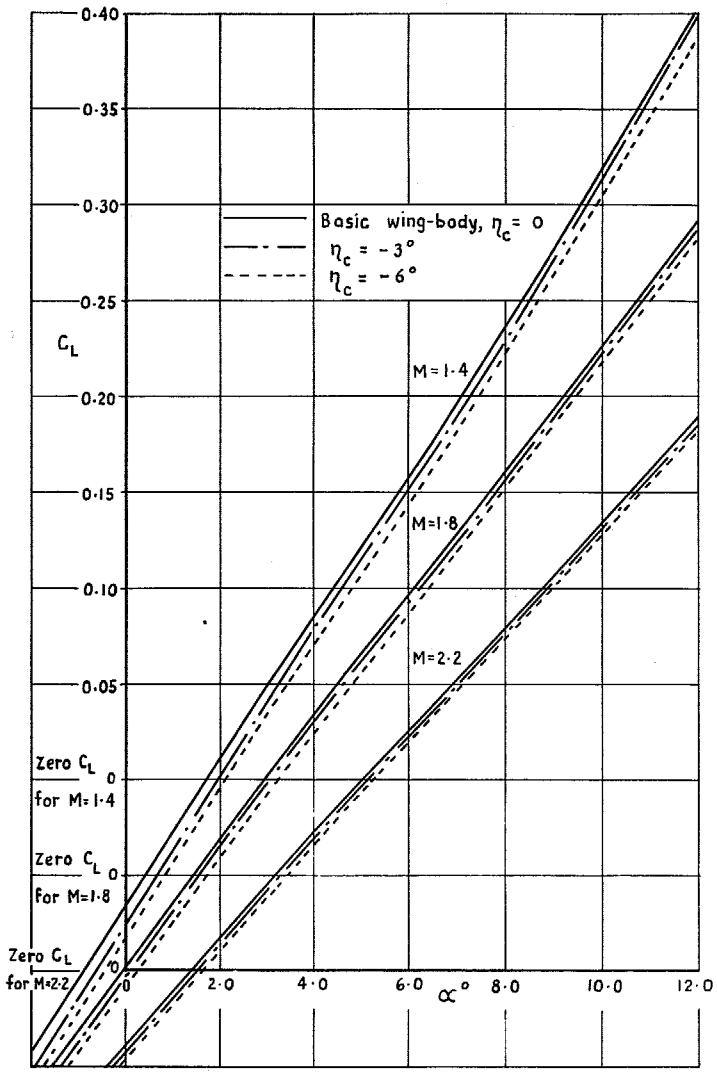

FIG. 17. Effect of inboard controls as elevators on lift at supersonic speeds.

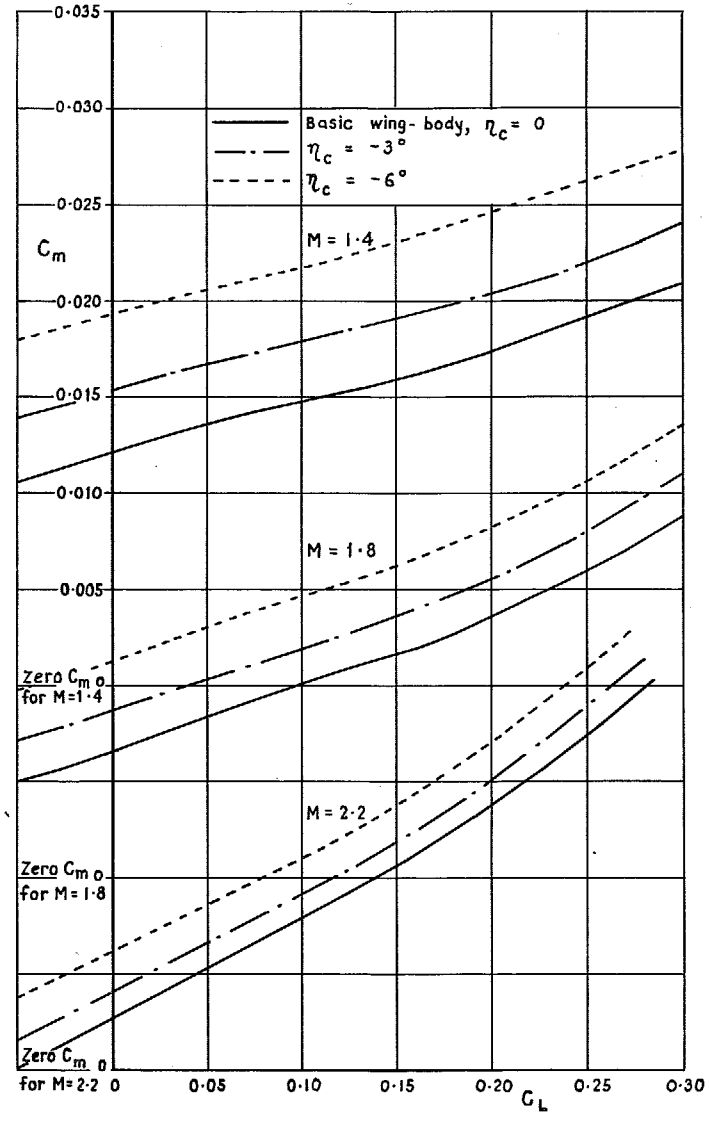

FIG. 18. Effect of inboard controls as elevators on pitching moment at supersonic speeds.

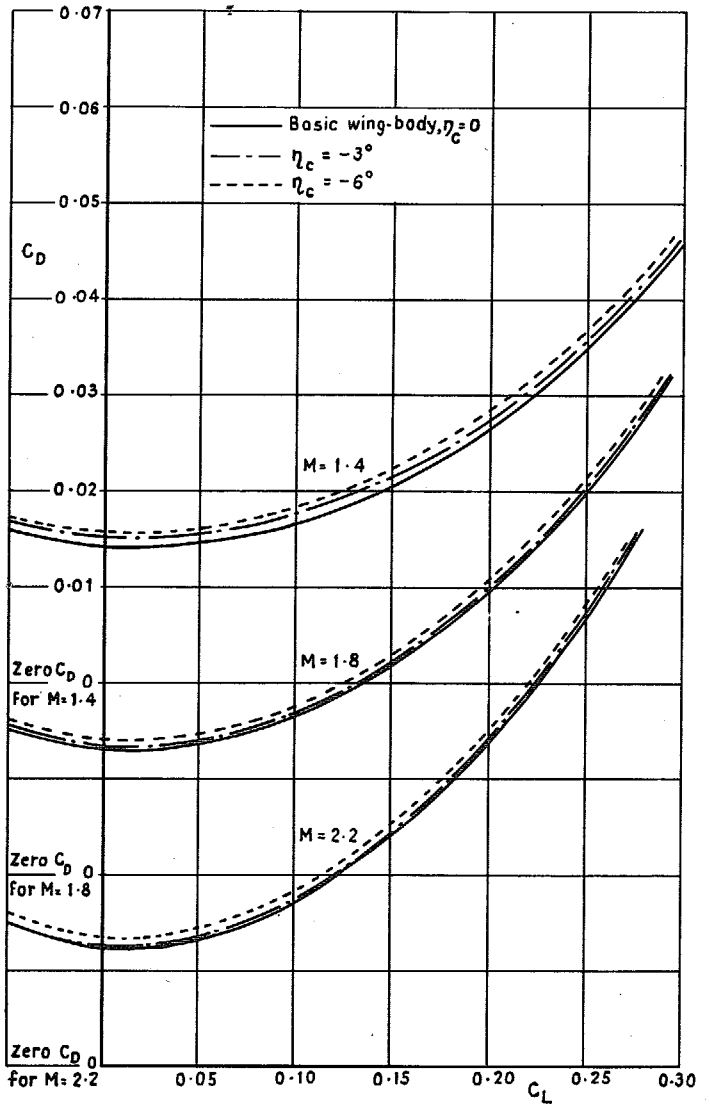

FIG. 19. Effect of inboard controls as elevators on drag at supersonic speeds.

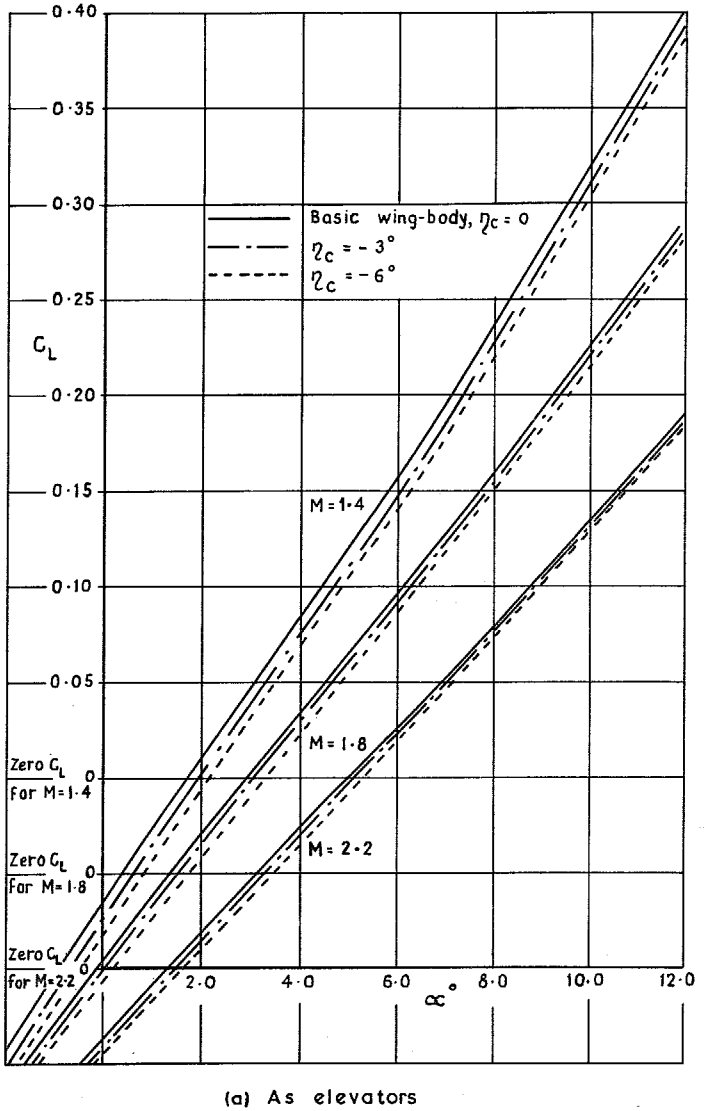

(a) As elevators

FIG. 20. Effect of outboard controls on lift at supersonic speeds.

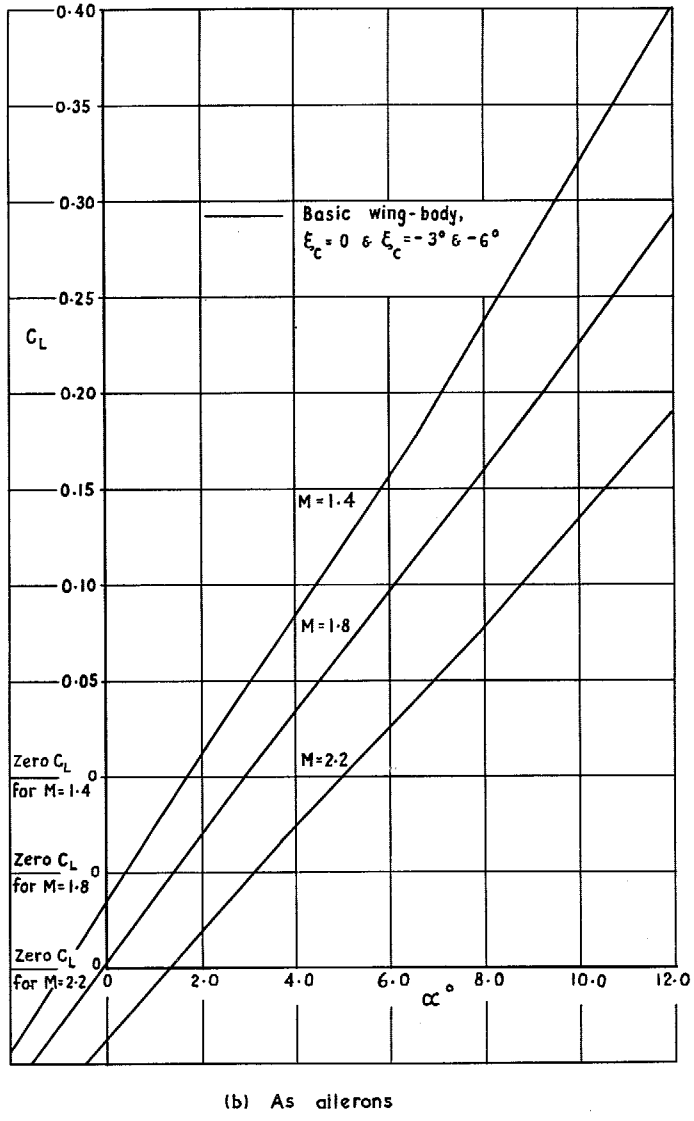

(b) As ailerons

FIG. 20 (*contd.*)

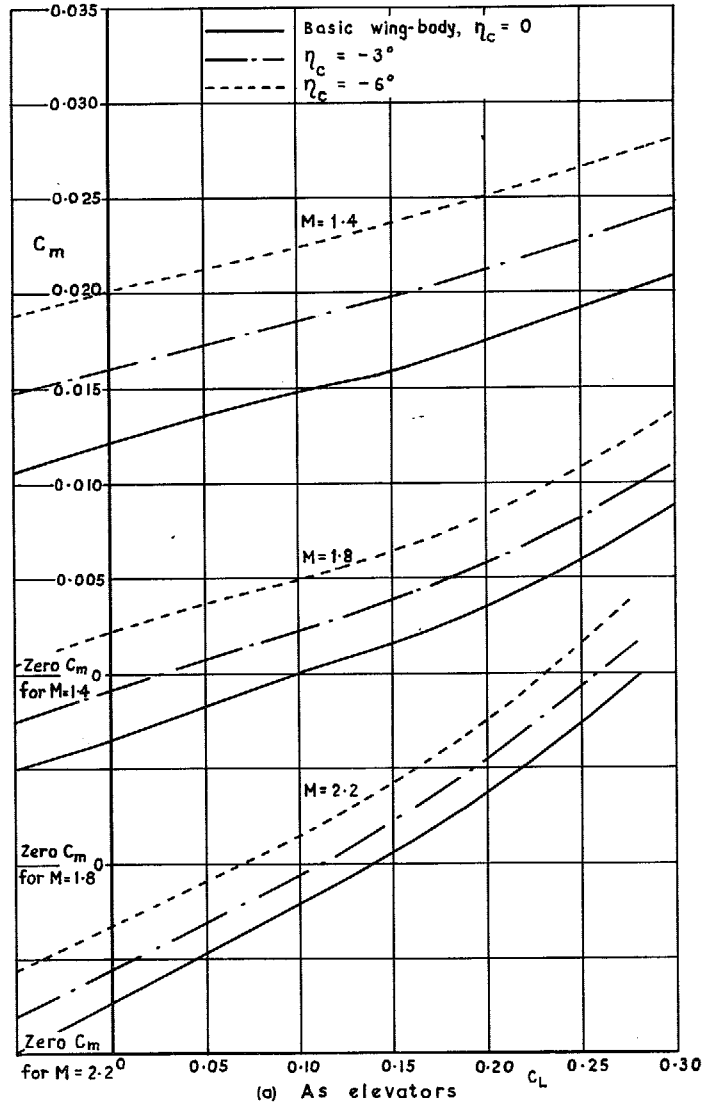

(a) As elevators

FIG. 21. Effect of outboard controls on pitching moment at supersonic speeds.

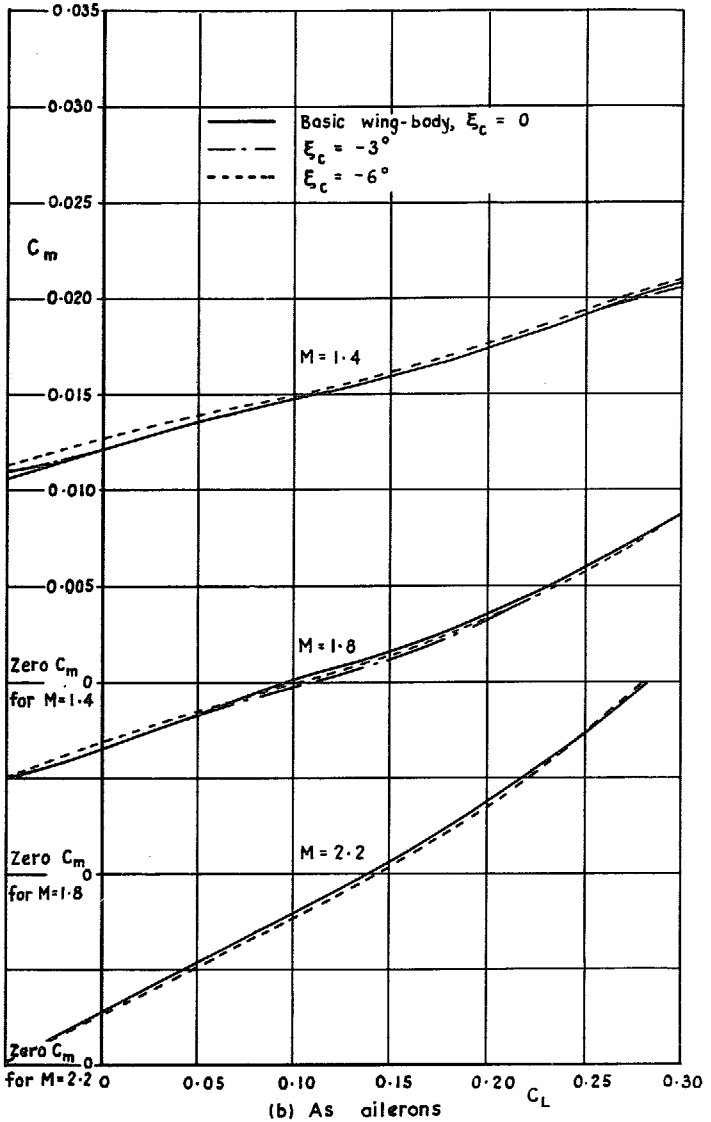

FIG. 21 (*contd.*)

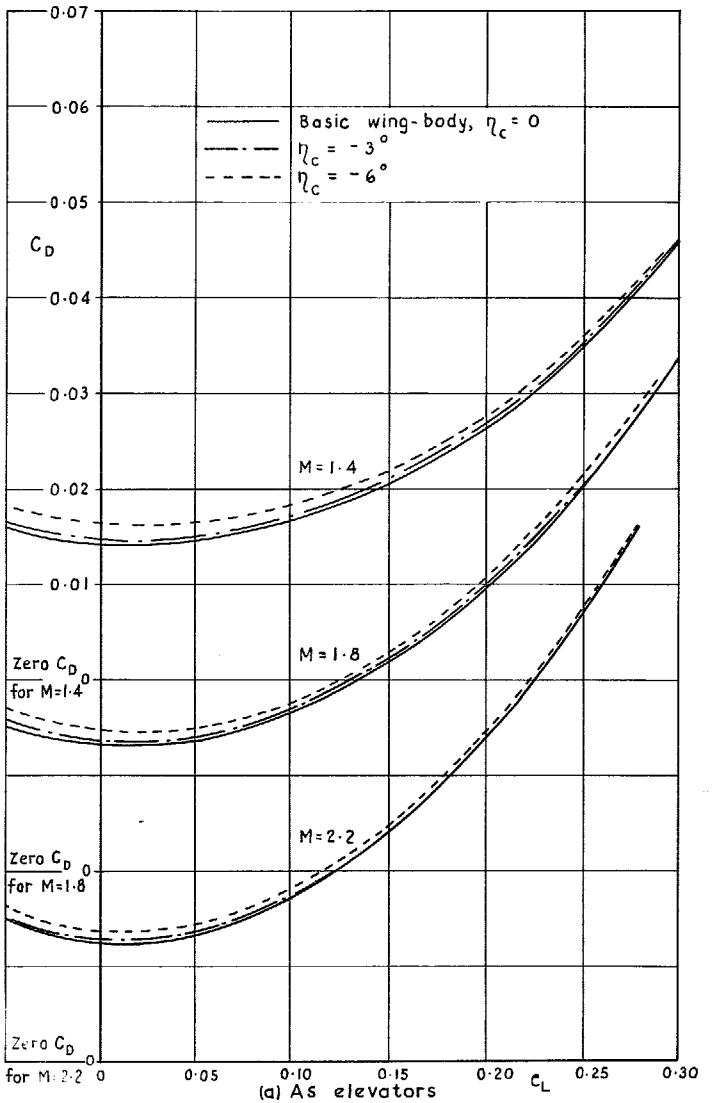

FIG. 22. Effect of outboard controls on drag at supersonic speeds.

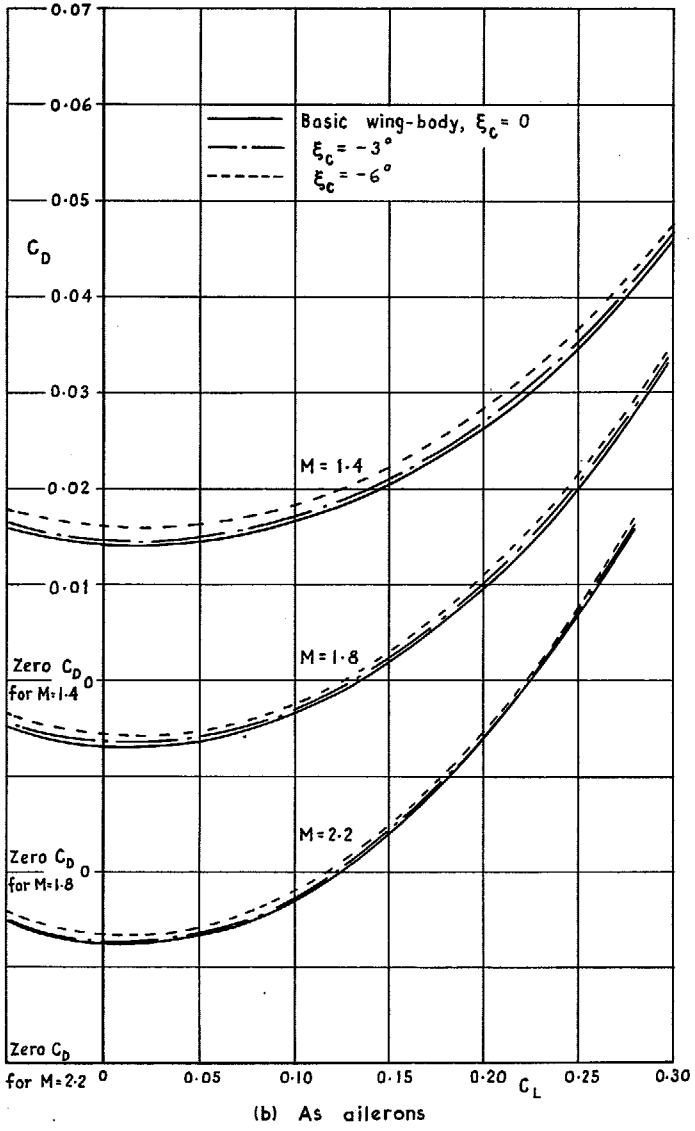

(b) As ailerons

FIG. 22 (*contd.*)

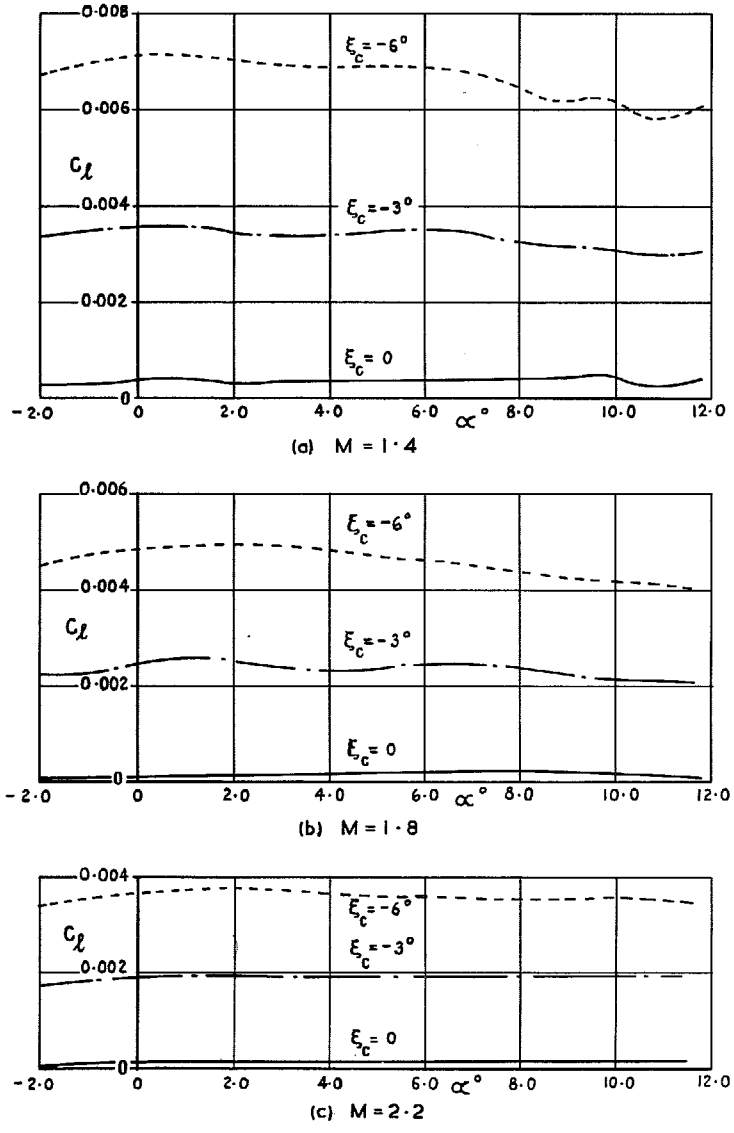

(a) M = 1·4

(b) M = 1·8

(c) M = 2·2

FIG. 23. Effect of outboard controls as ailerons on rolling moment at supersonic speeds.

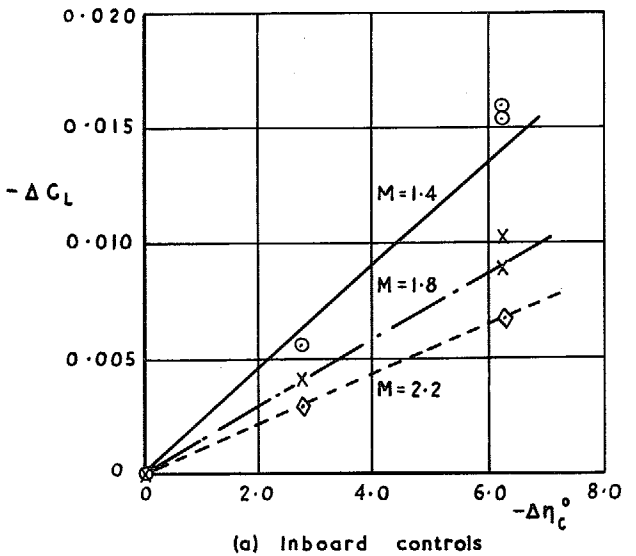

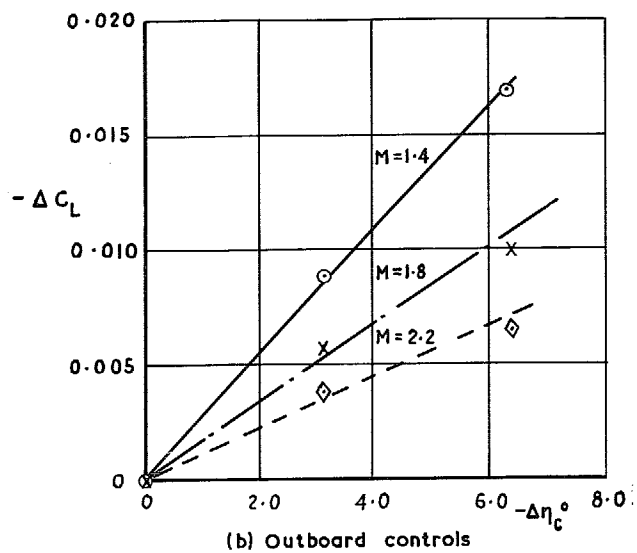

FIG. 24. Incremental lift coefficients due to controls $\alpha = 2{\cdot}90°$.

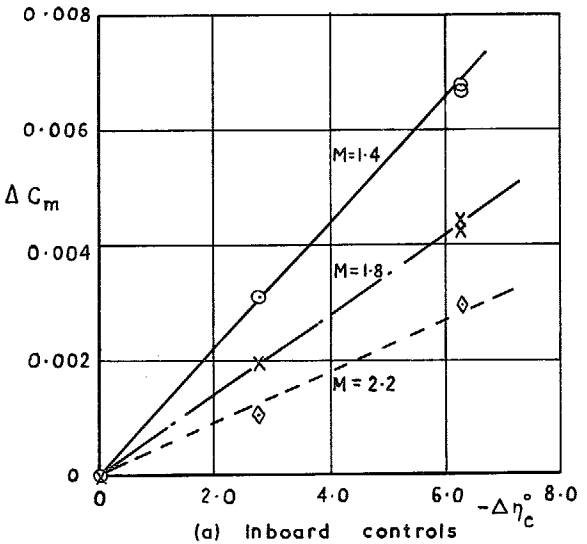

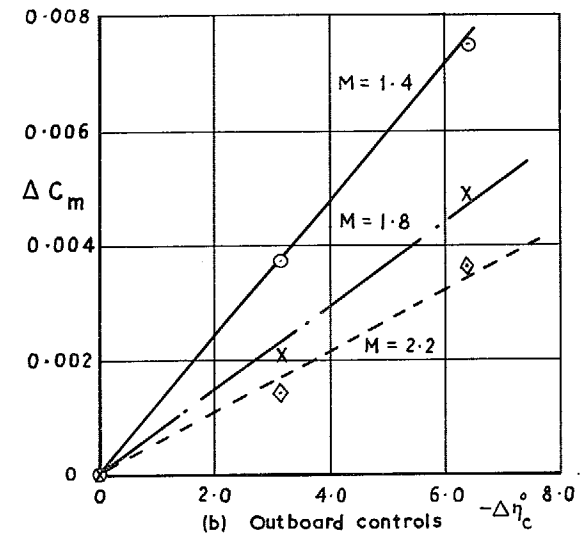

FIG. 25. Incremental pitching moment coefficients due to controls, $\alpha = 2{\cdot}90°$.

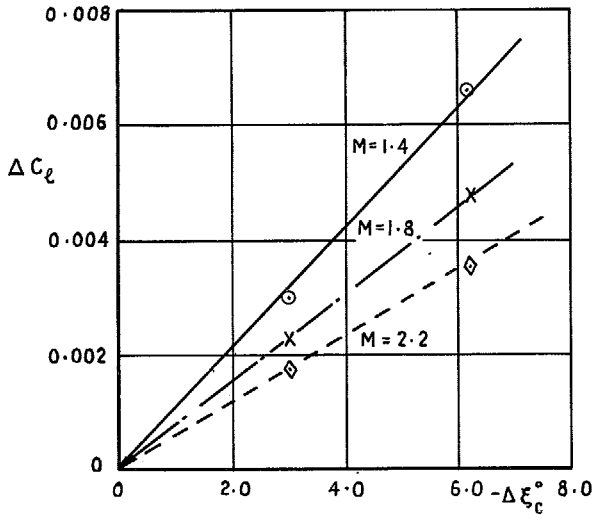

FIG. 26. Incremental rolling moment due to outboard controls, $\alpha = 2{\cdot}90°$.

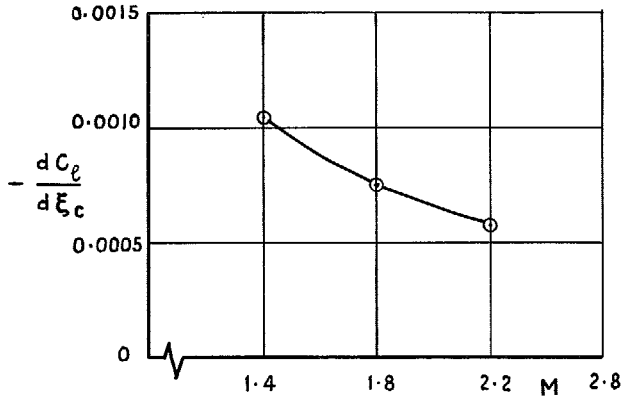

FIG. 27. Rolling moment effectiveness of outboard controls, $\alpha = 2{\cdot}90°$.

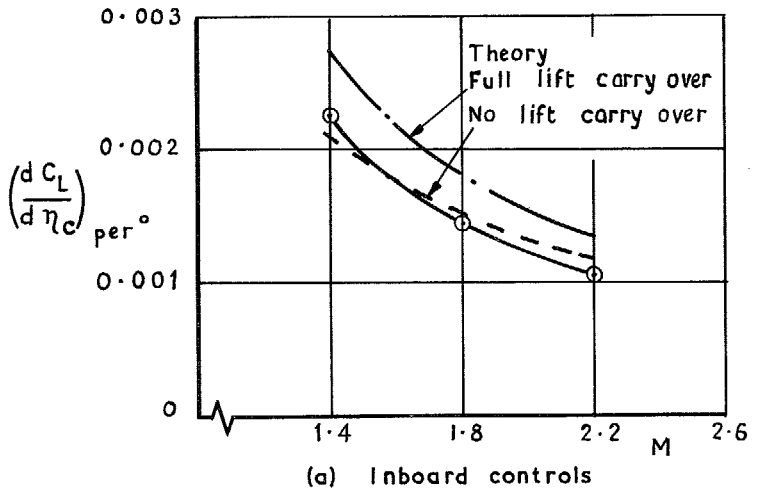

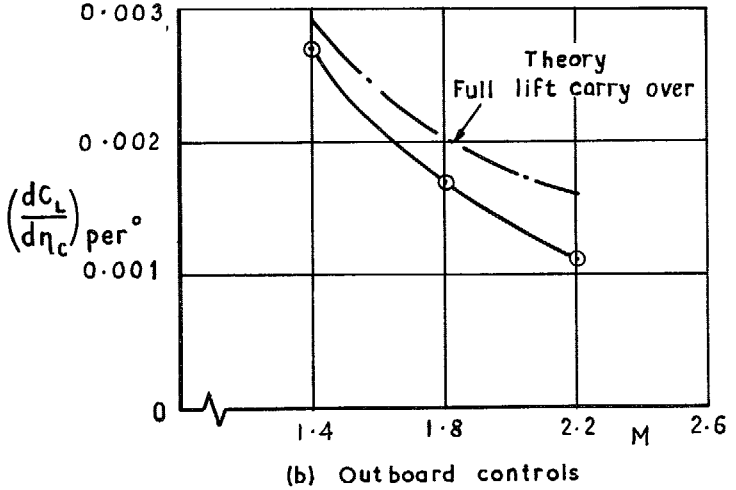

FIG. 28. Lift effectiveness of controls, $\alpha = 2{\cdot}90°$.

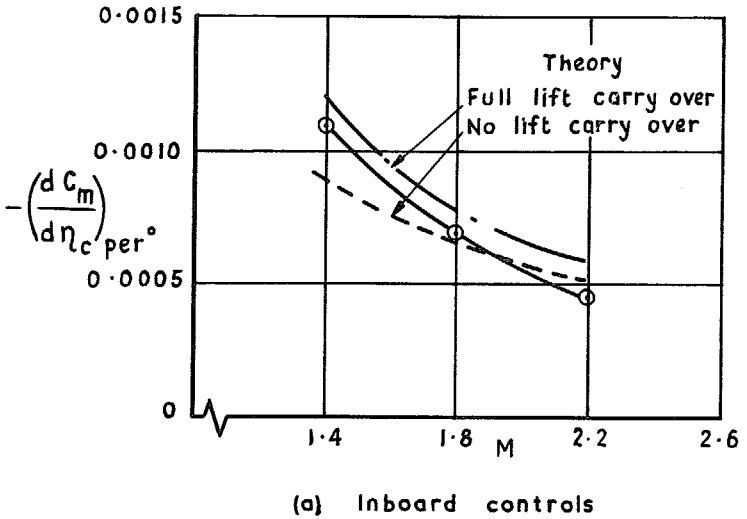

(a) Inboard controls

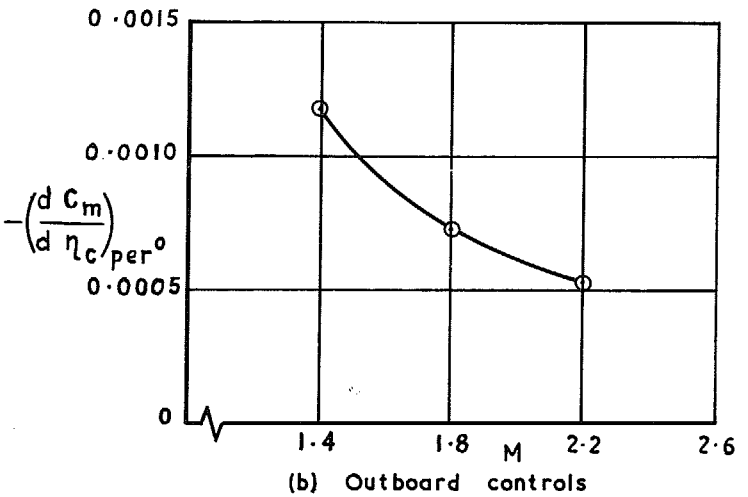

(b) Outboard controls

FIG. 29. Pitching moment effectiveness of controls, $\alpha = 2{\cdot}90°$.

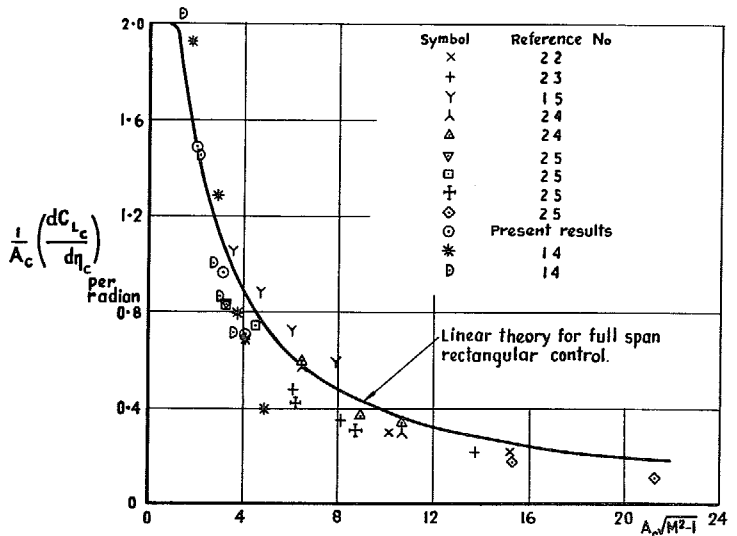

(a) Experimental values not corrected for control thickness or body interference

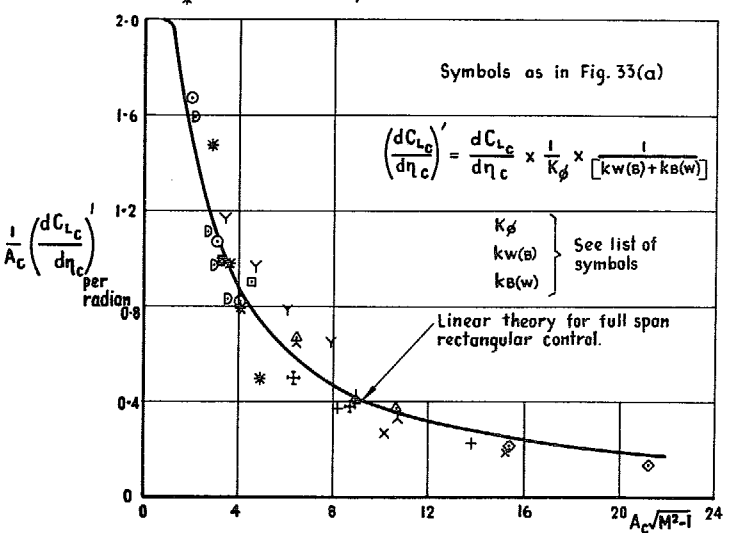

(b) Experimental values corrected for control thickness and body interference

FIG. 30. Lift effectiveness correlation for various rectangular controls.

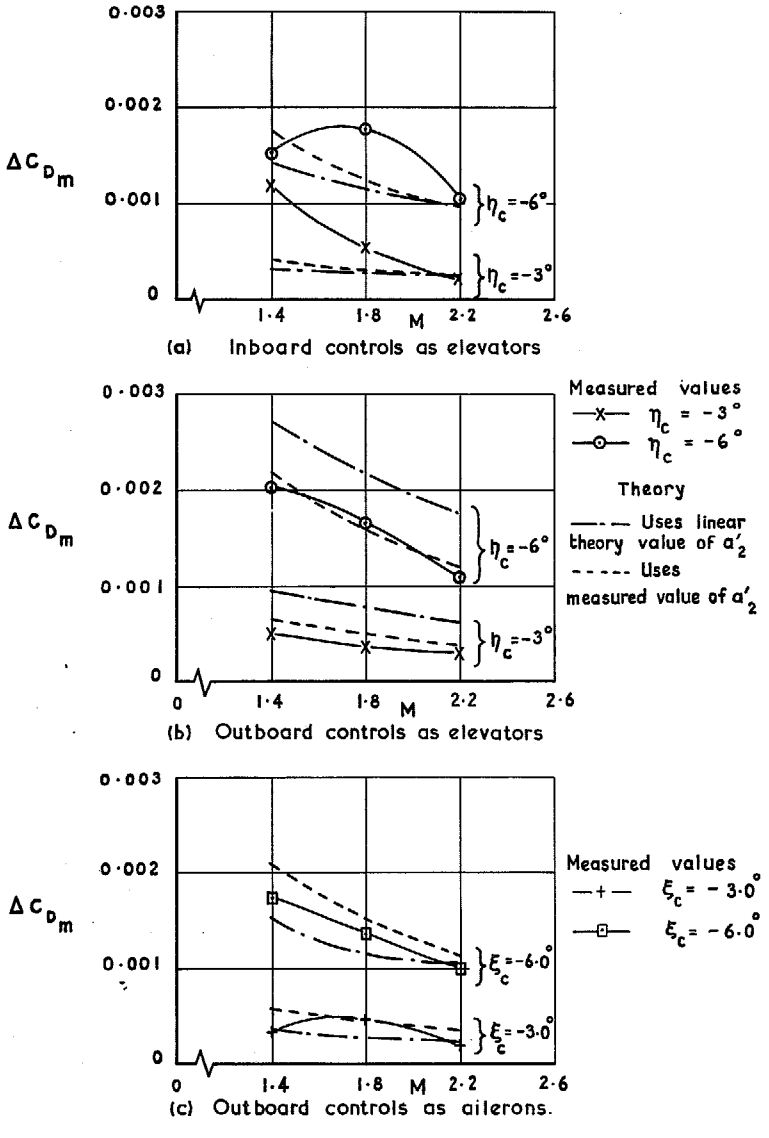

FIG. 31. Minimum drag increment due to control deflection.

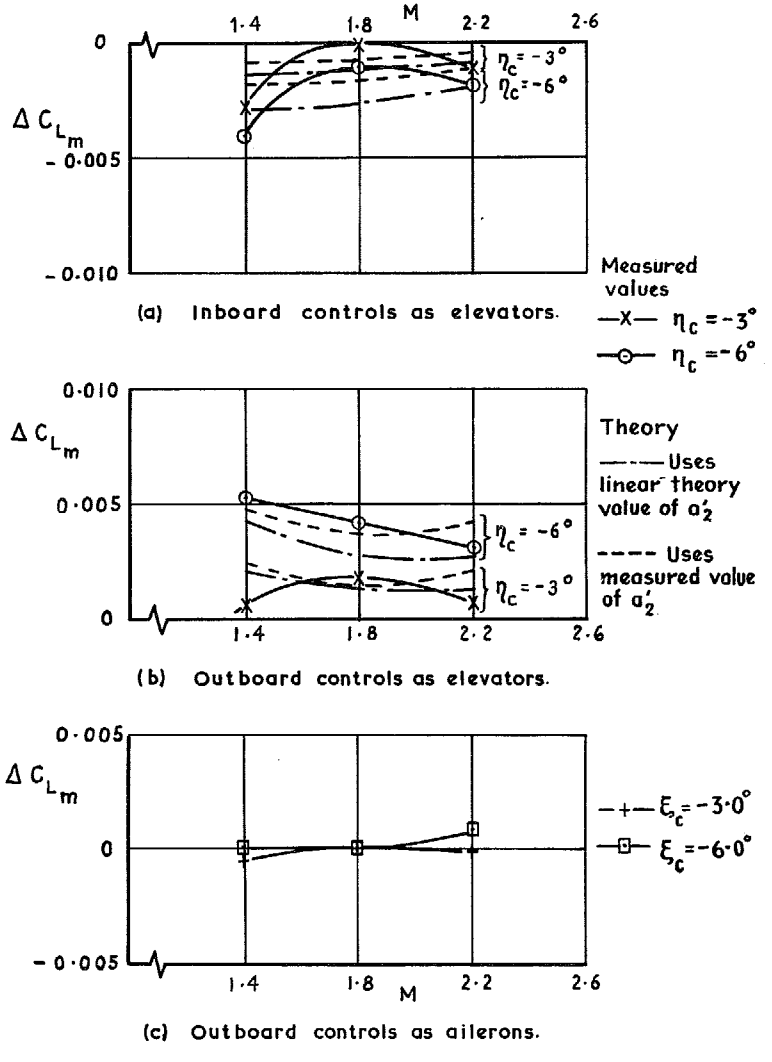

FIG. 32. Increment in lift at minimum drag due to control deflection.

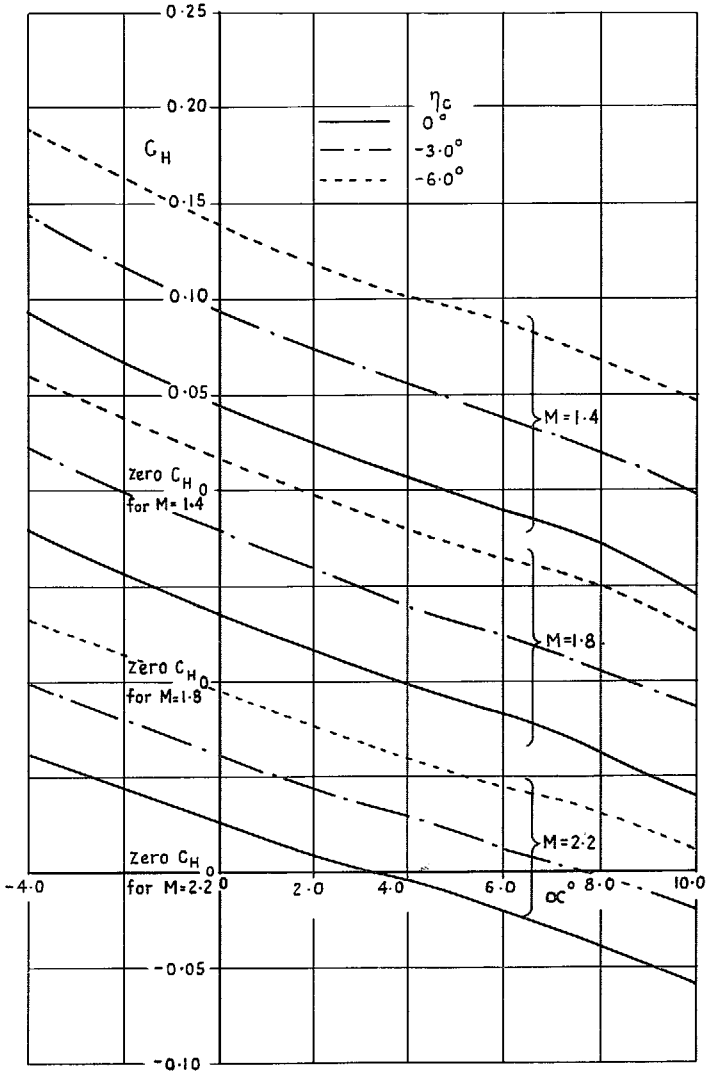

FIG. 33. Effect of incidence and control setting on inboard control hinge moments.

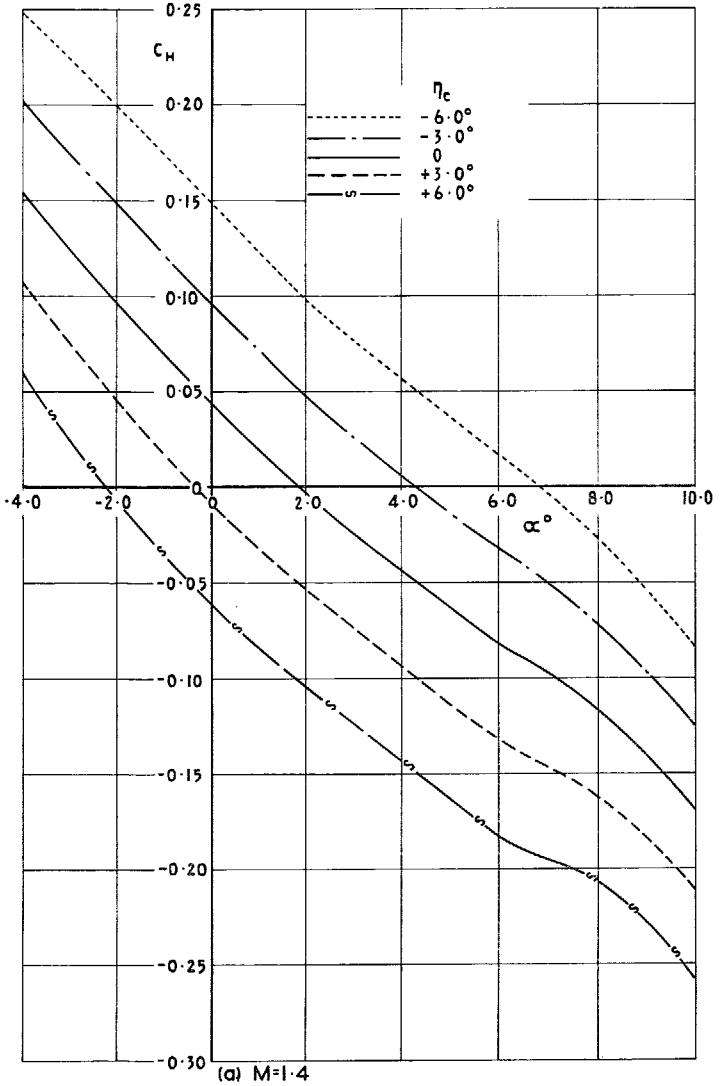

FIG. 34. Effect of incidence and control setting on outboard control hinge moments.

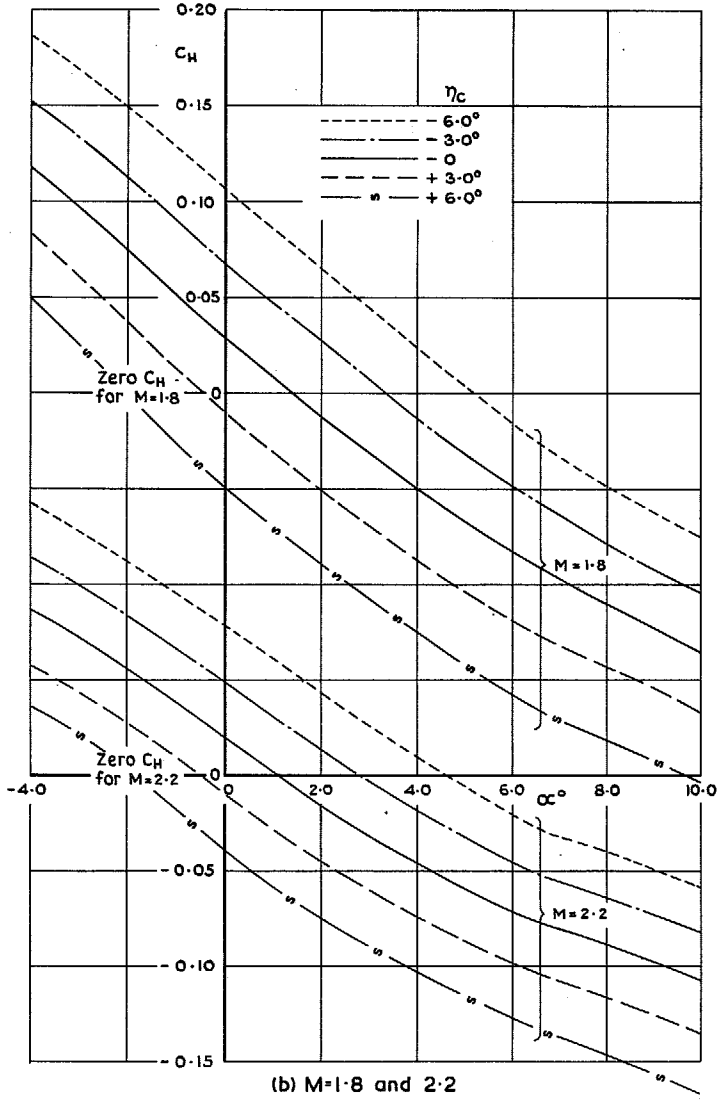

(b) M=1·8 and 2·2

FIG. 34 (*contd.*). Effect of incidence and control setting on outboard control hinge moments.

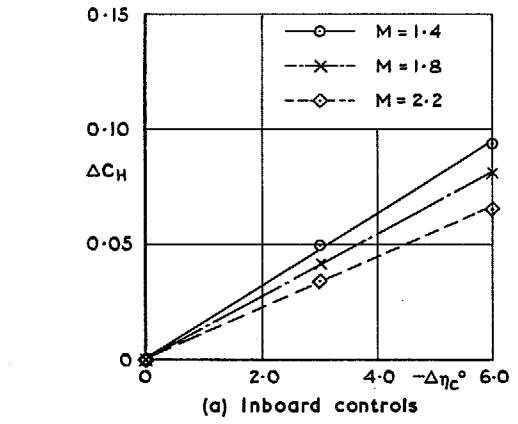

(a) Inboard controls

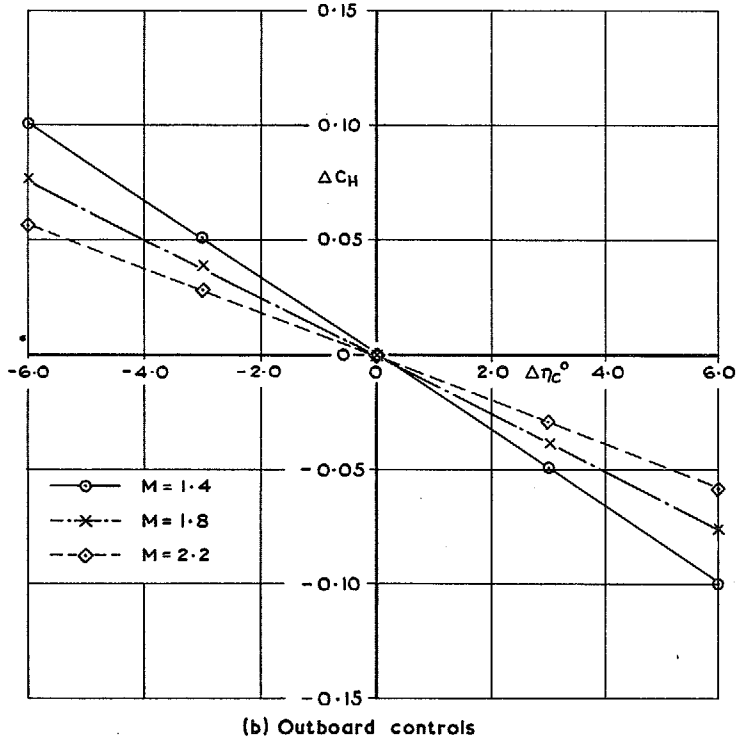

(b) Outboard controls

FIG. 35. Variation of control hinge moment coefficient with control setting, $\alpha = 2{\cdot}90°$.

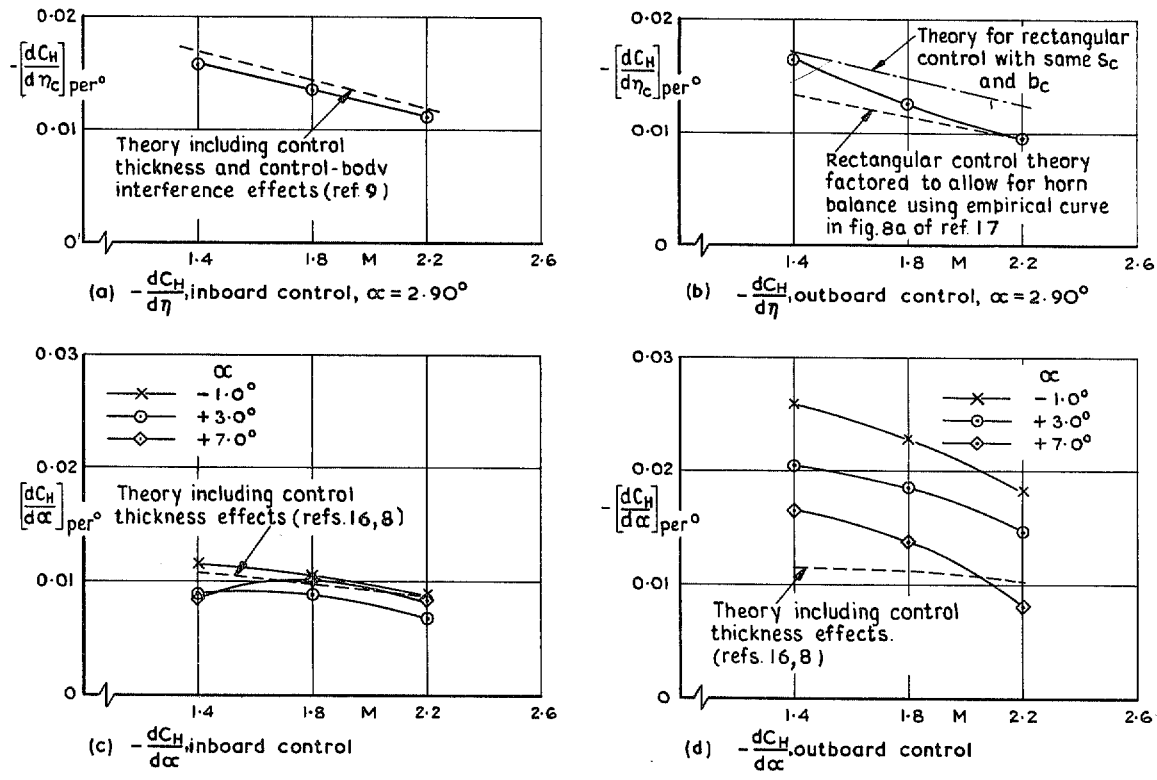

FIG. 36. Variation with Mach No. of the hinge moment derivatives $\frac{dC_H}{d\eta}$ and $\frac{dC_H}{d\alpha}$.

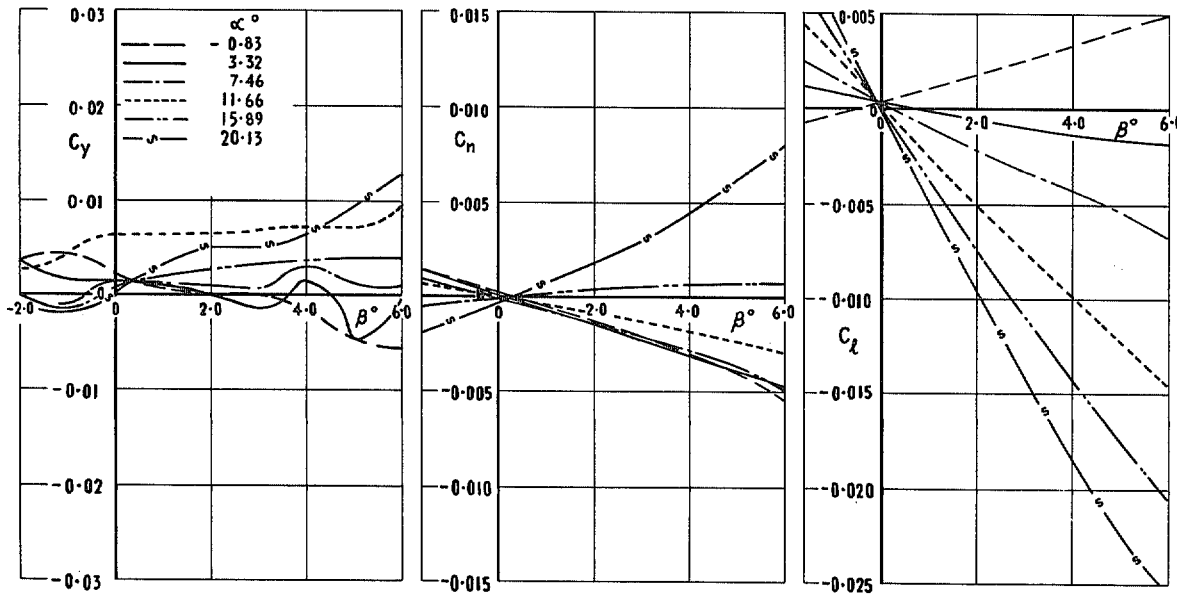

FIG. 37. Variation of C_y, C_n and C_l with β for the basic wing-body at subsonic speeds ($M = 0{\cdot}275$).

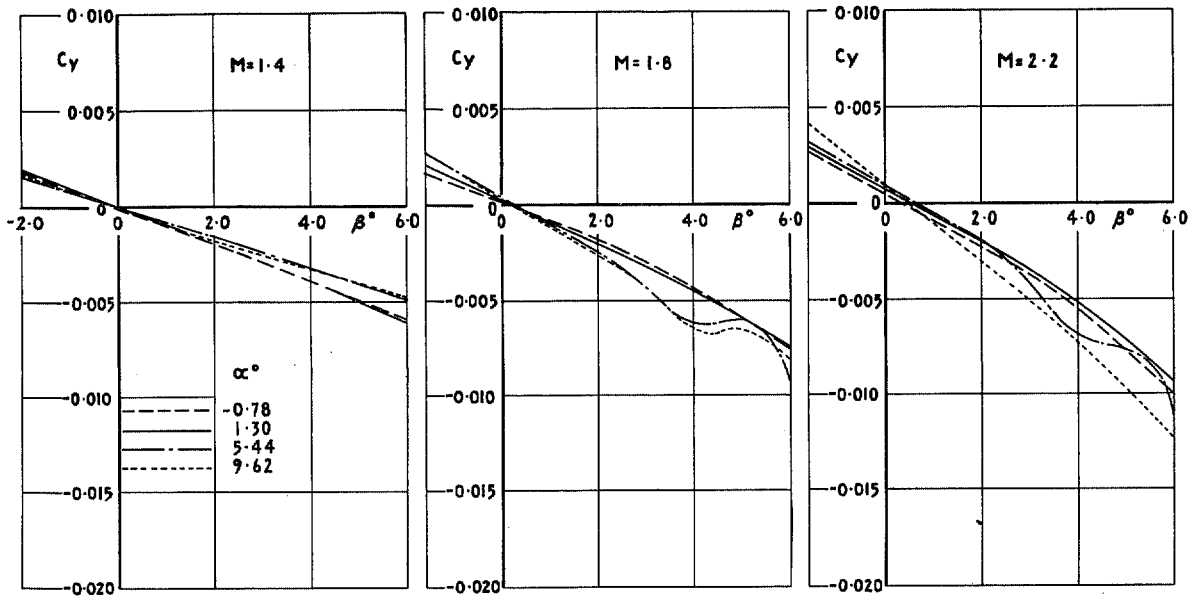

FIG. 38. Variation of C_y with β for the basic wing-body at supersonic speeds.

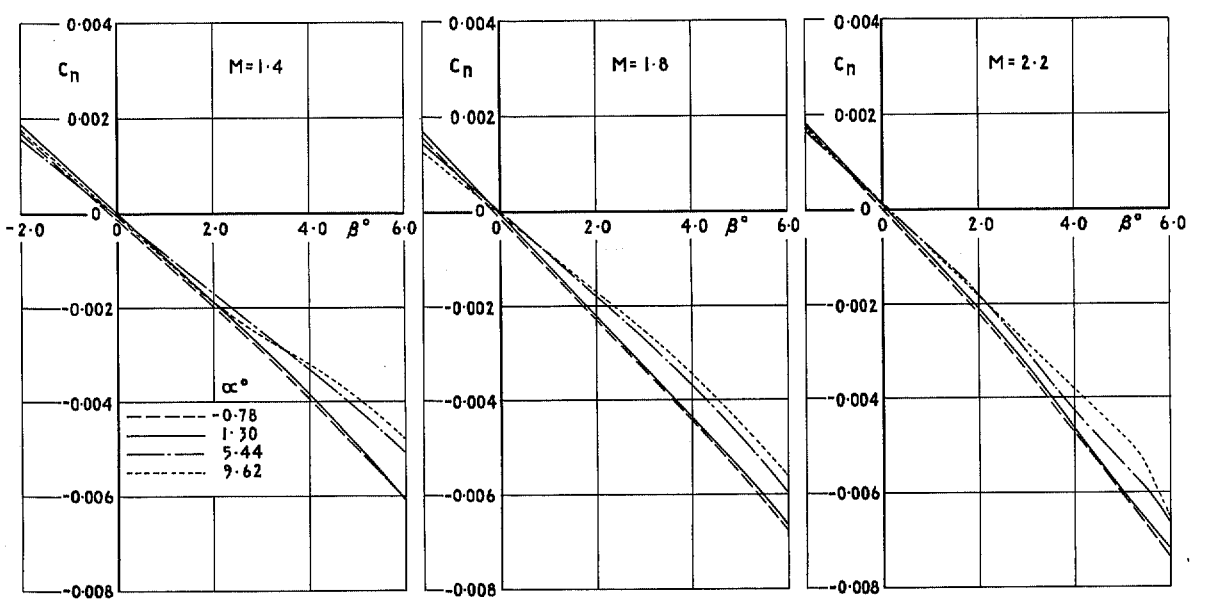

FIG. 39. Variation of C_n with β for the basic wing-body at supersonic speeds.

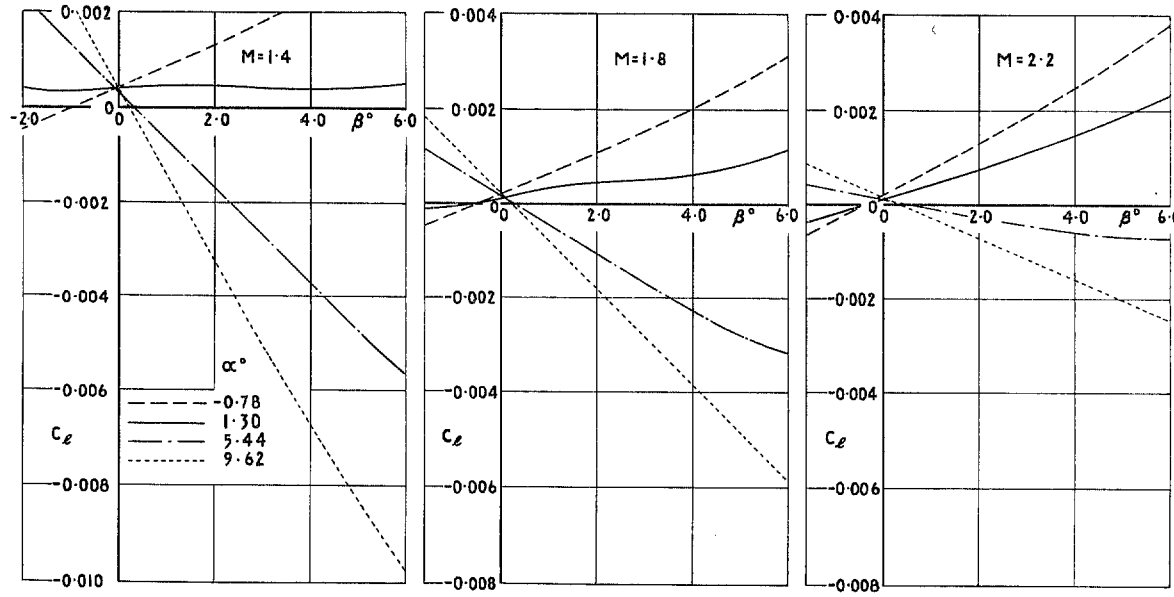

FIG. 40. Variation of C_l with β for the basic wing-body at supersonic speeds.

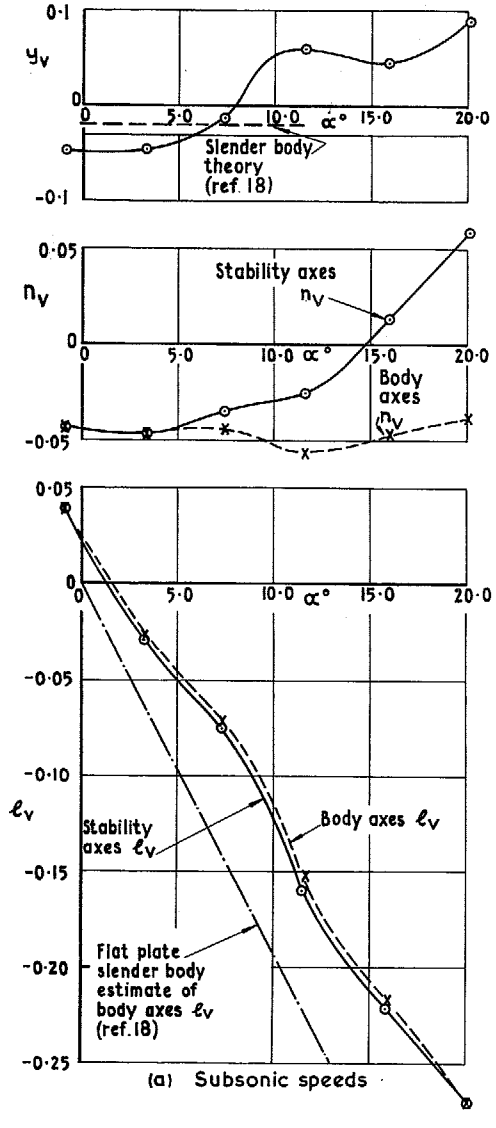

FIG. 41. Effect of incidence and Mach No. on the derivatives y_v, n_v and l_v for the basic wing-body.

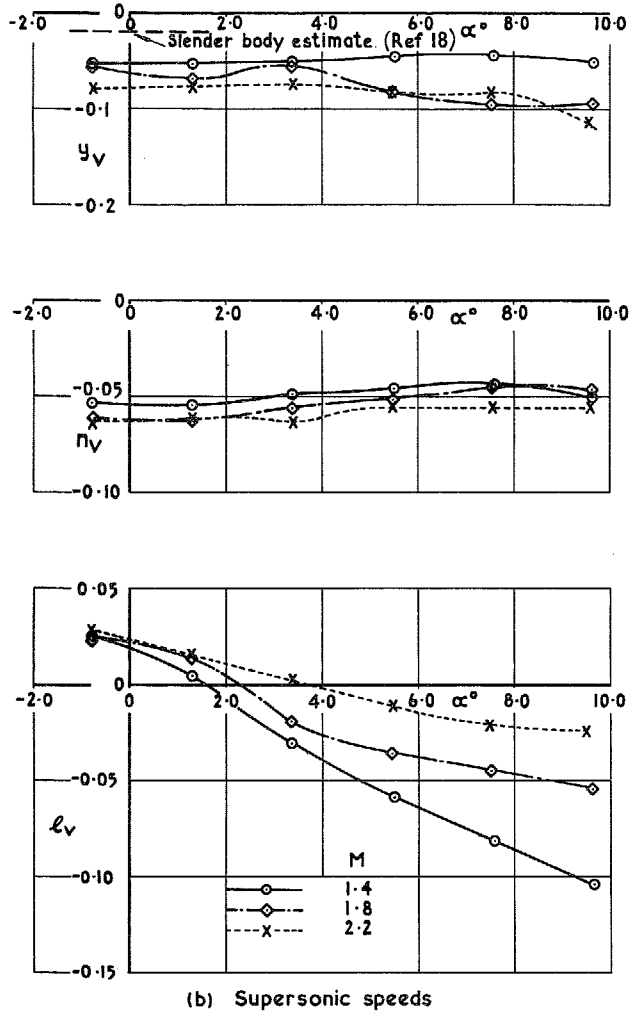

FIG. 41 (*contd.*)

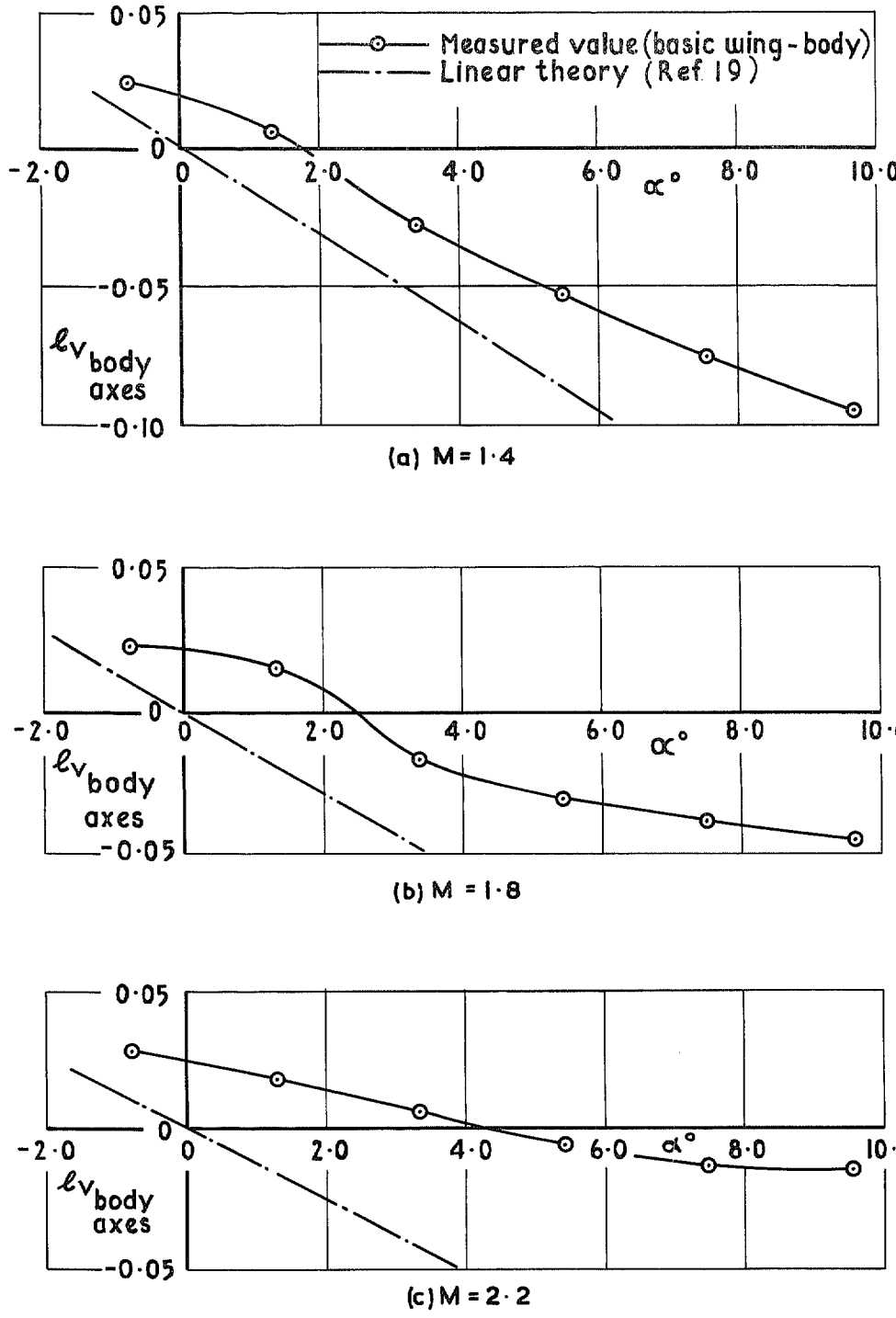

FIG. 42. Comparison of experimental and theoretical values of body axes l_v at supersonic speeds.

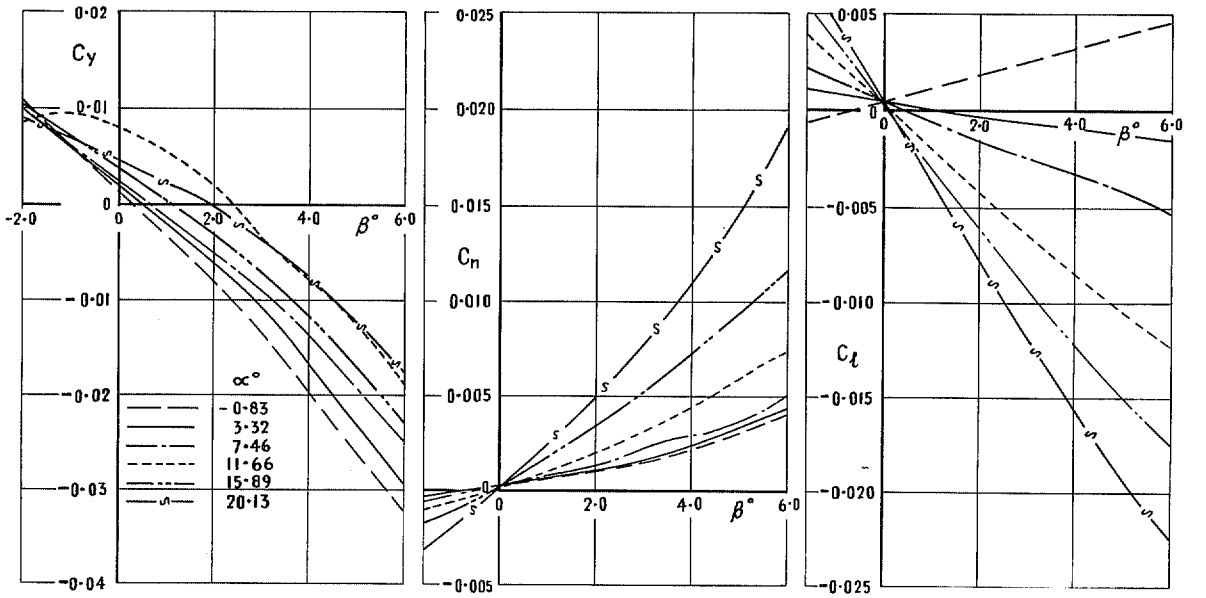

FIG. 43. Variation of C_y, C_n and C_l with β for the wing-body with fin (long shroud) at subsonic speeds ($M = 0{\cdot}275$).

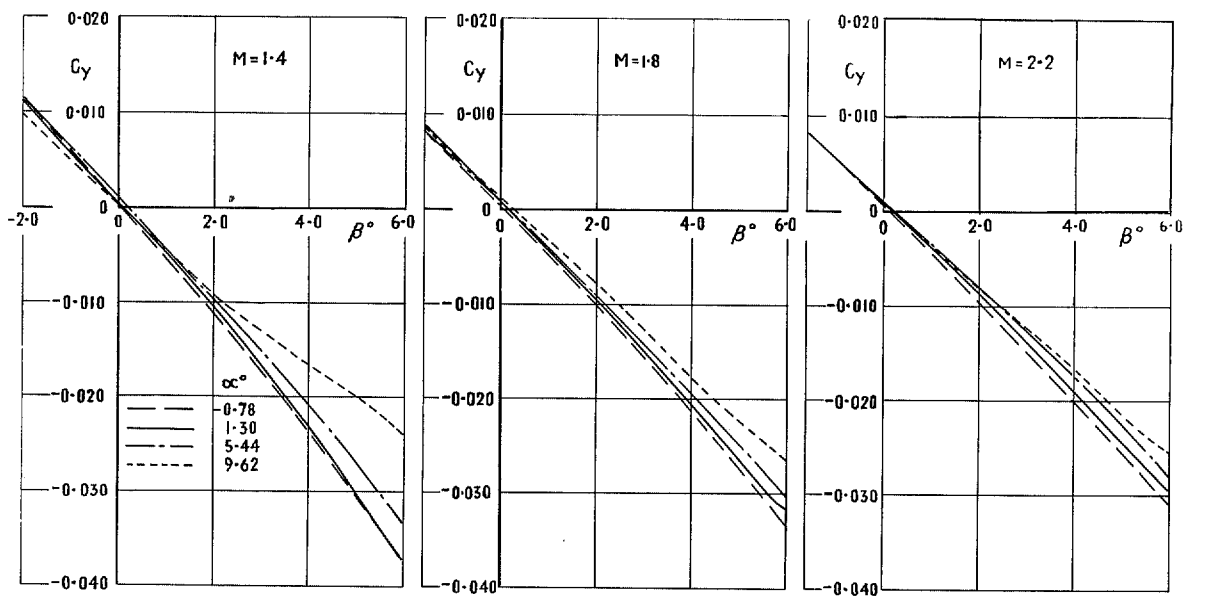

FIG. 44. Variation of C_y with β for the wing-body with fin (long shroud) at supersonic speeds.

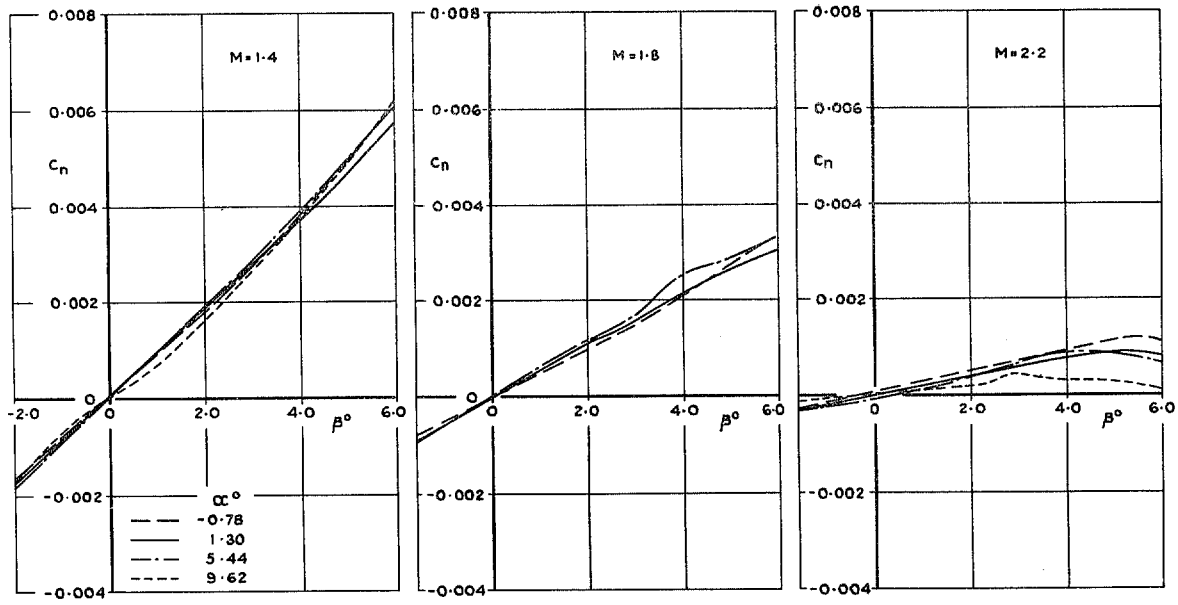

FIG. 45. Variation of C_n with β for the wing-body with fin (long shroud) at supersonic speeds.

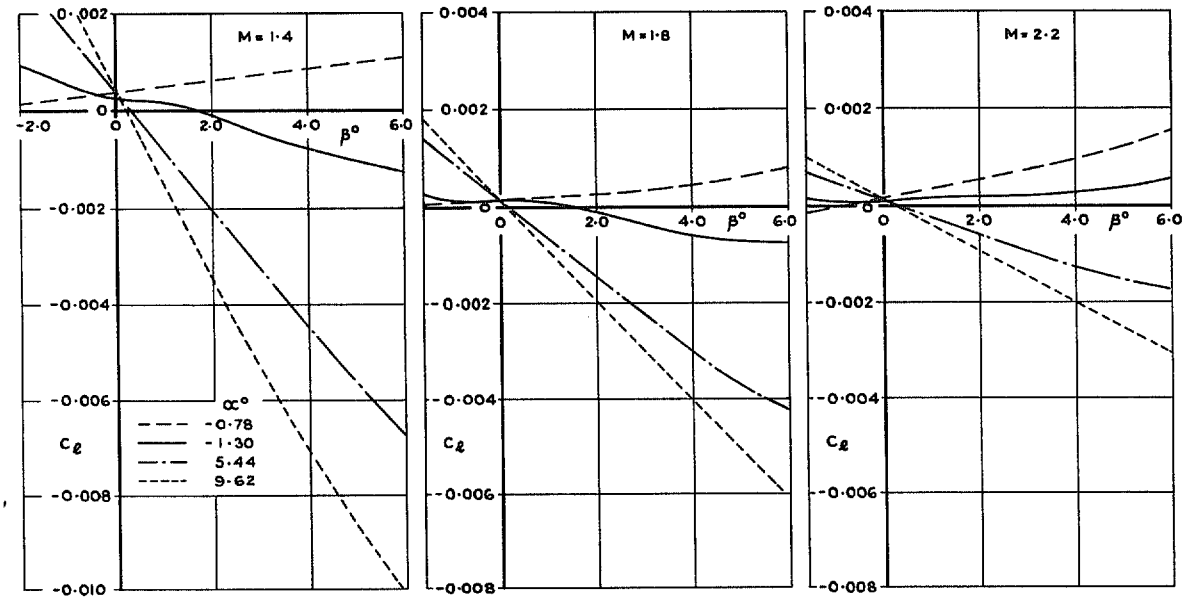

FIG. 46. Variation of C_l with β for the wing-body with fin (long shroud) at supersonic speeds.

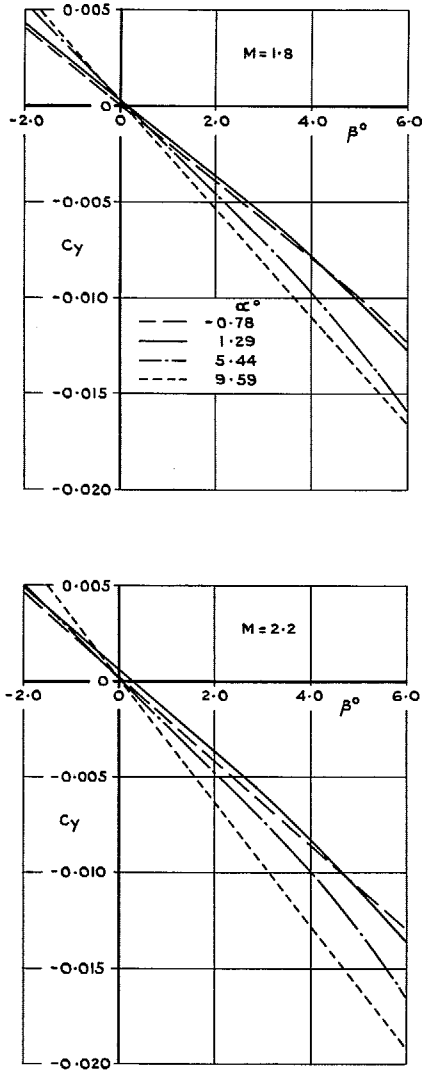

FIG. 47. Variation of C_y with β for the wing-body with nacelles at supersonic speeds.

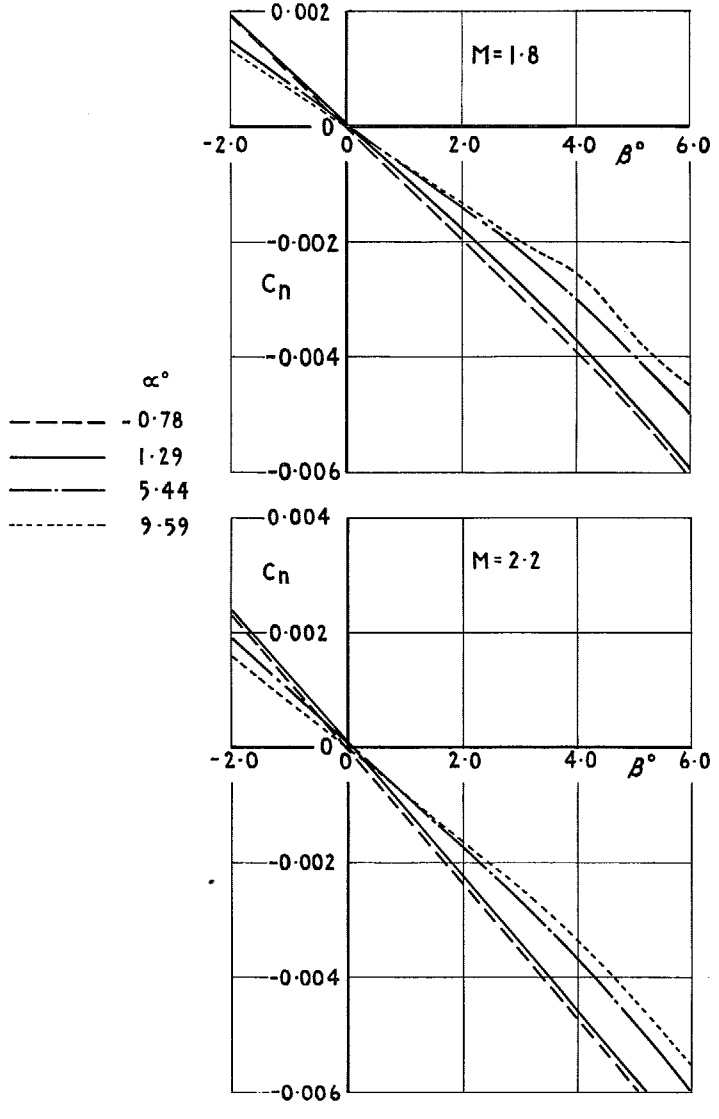

FIG. 48. Variation of C_n with β for the wing-body with nacelles at supersonic speeds.

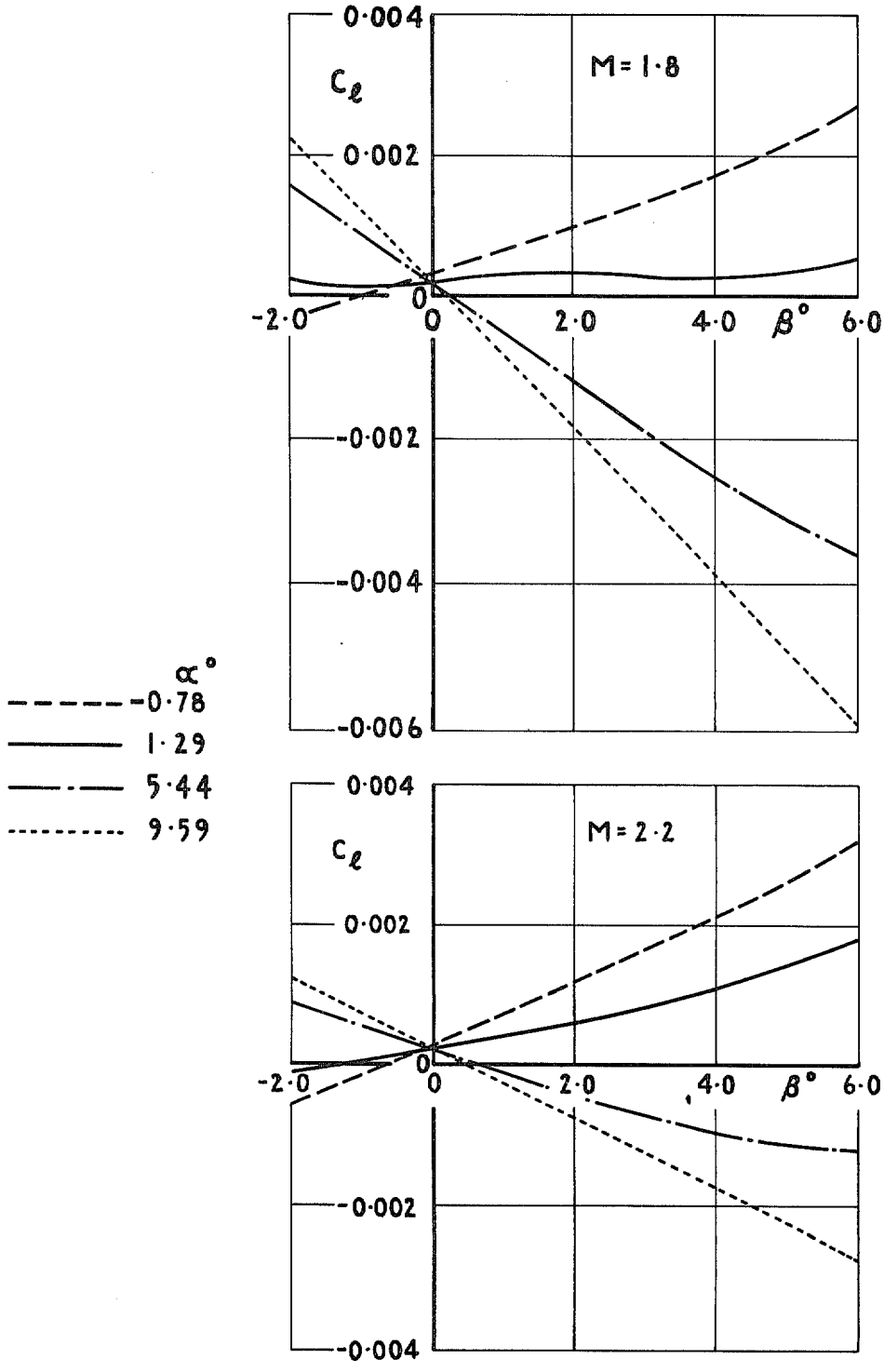

FIG. 49. Variation of C_l with β for the wing-body with nacelles at supersonic speeds.

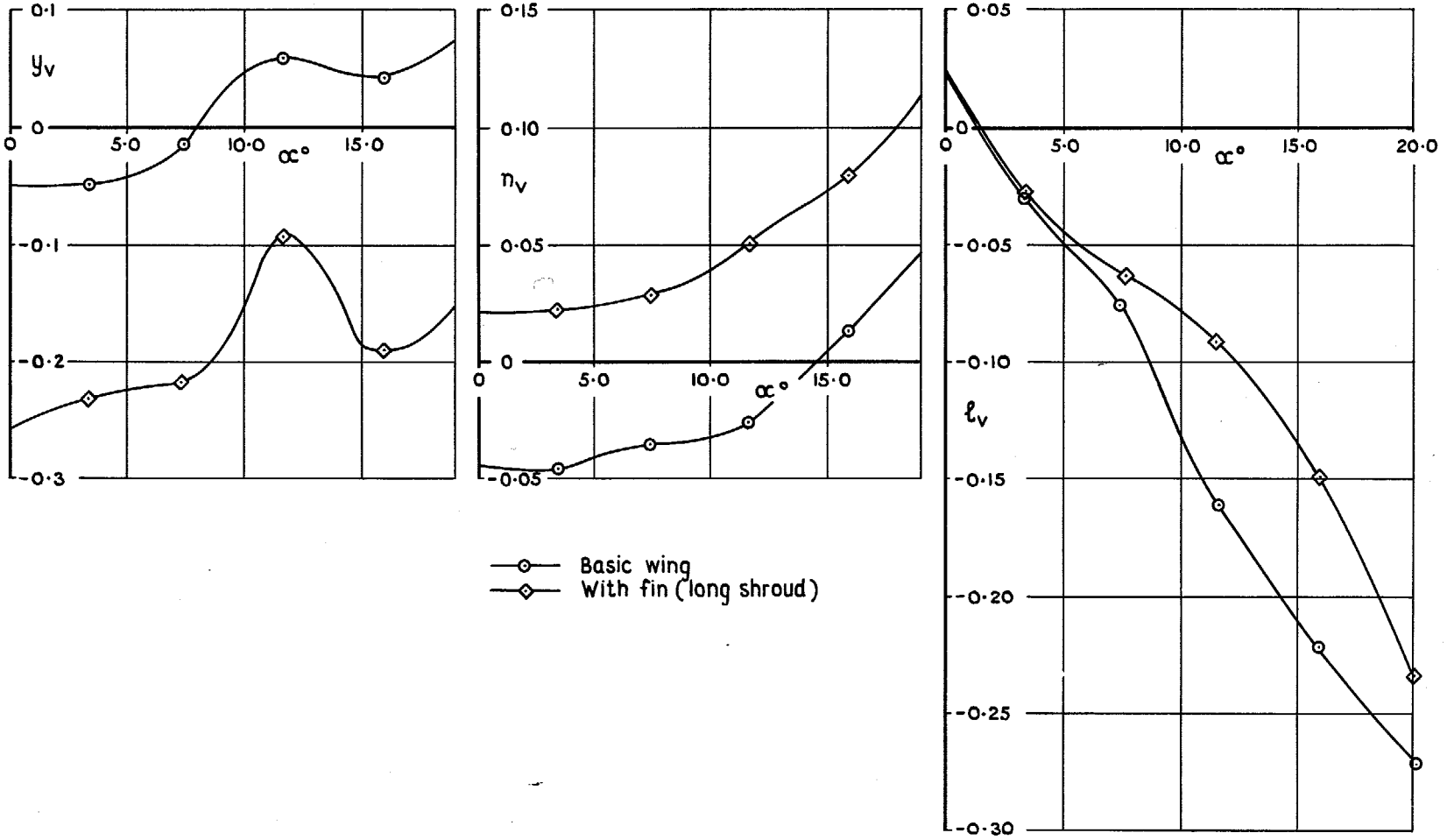

FIG. 50. Effect of fin on y_v, n_v and l_v at subsonic speeds ($M = 0{\cdot}275$).

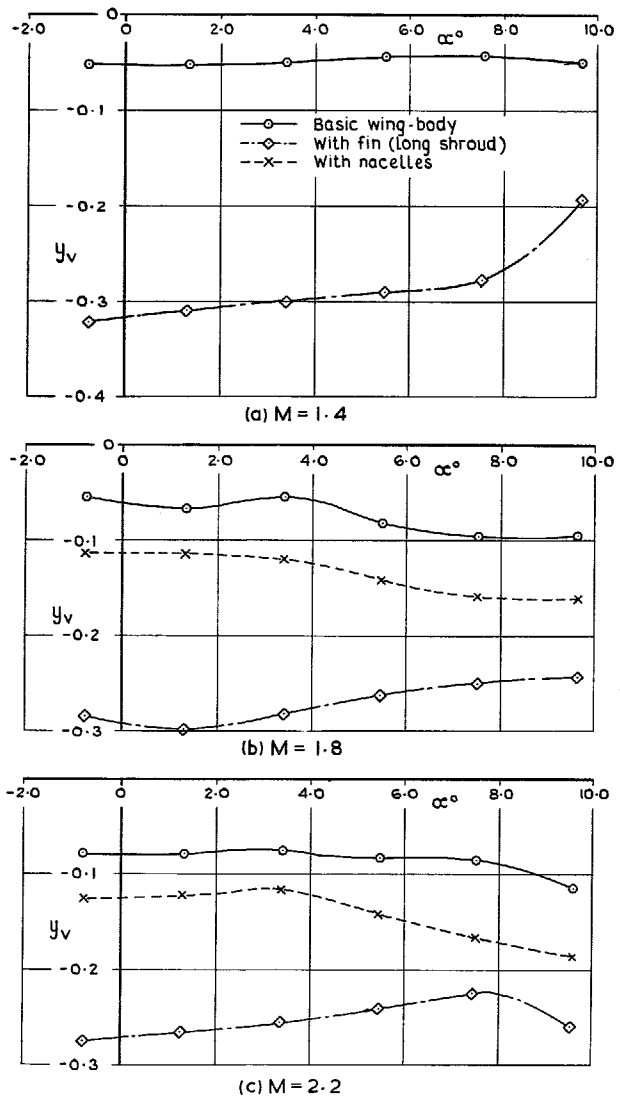

FIG. 51. Effect of fin and nacelles on y_v at supersonic speeds.

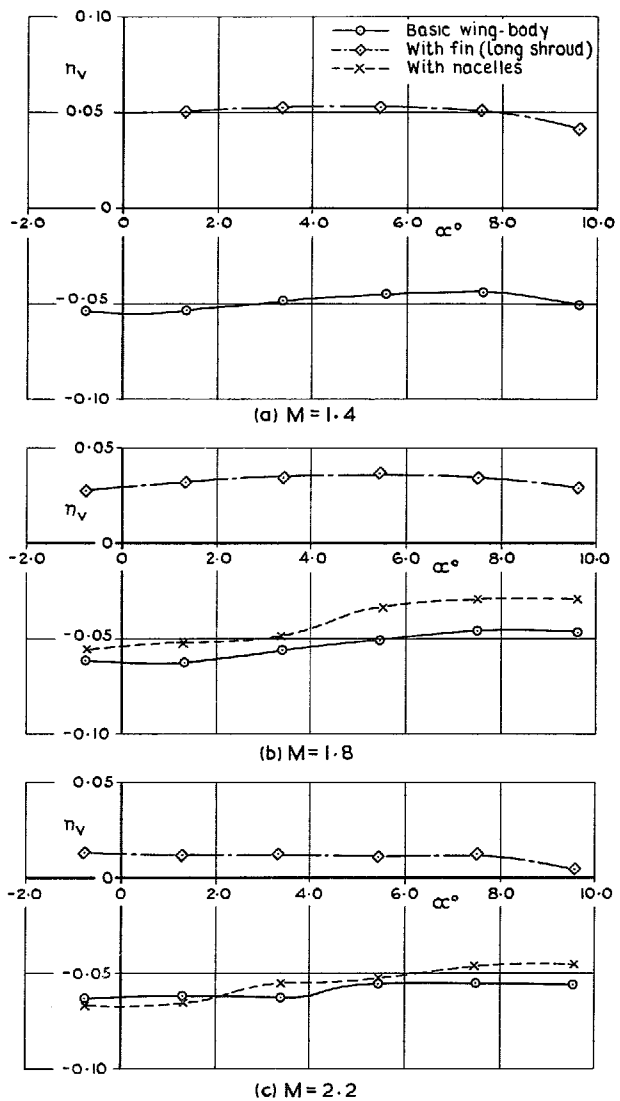

FIG. 52. Effect of fin and nacelles on n_v at supersonic speeds.

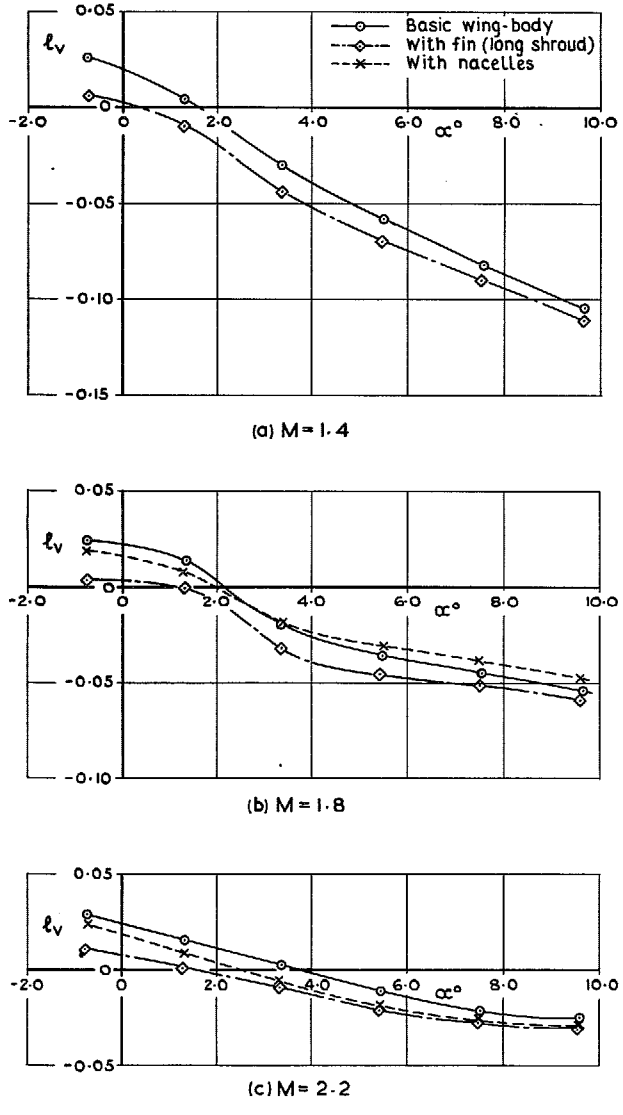

FIG. 53. Effect of fin and nacelles on l_v at supersonic speeds.

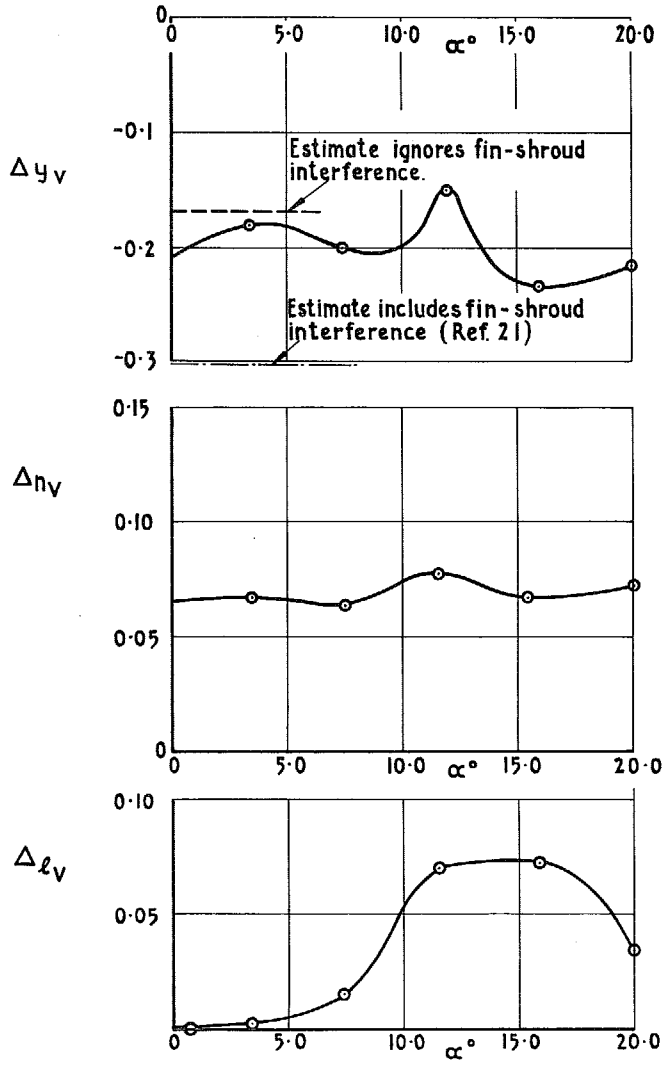

FIG. 54. Increments in y_v, n_v and l_v due to the fin at subsonic speeds ($M = 0{\cdot}275$).

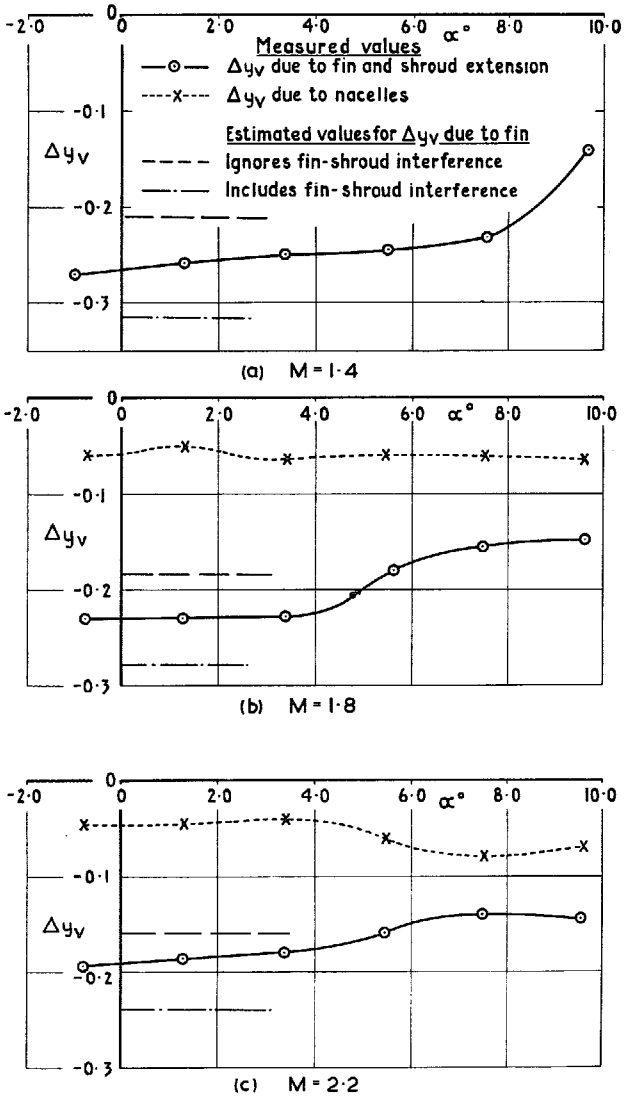

FIG. 55. Increments in y_v due to fin and nacelles at supersonic speeds.

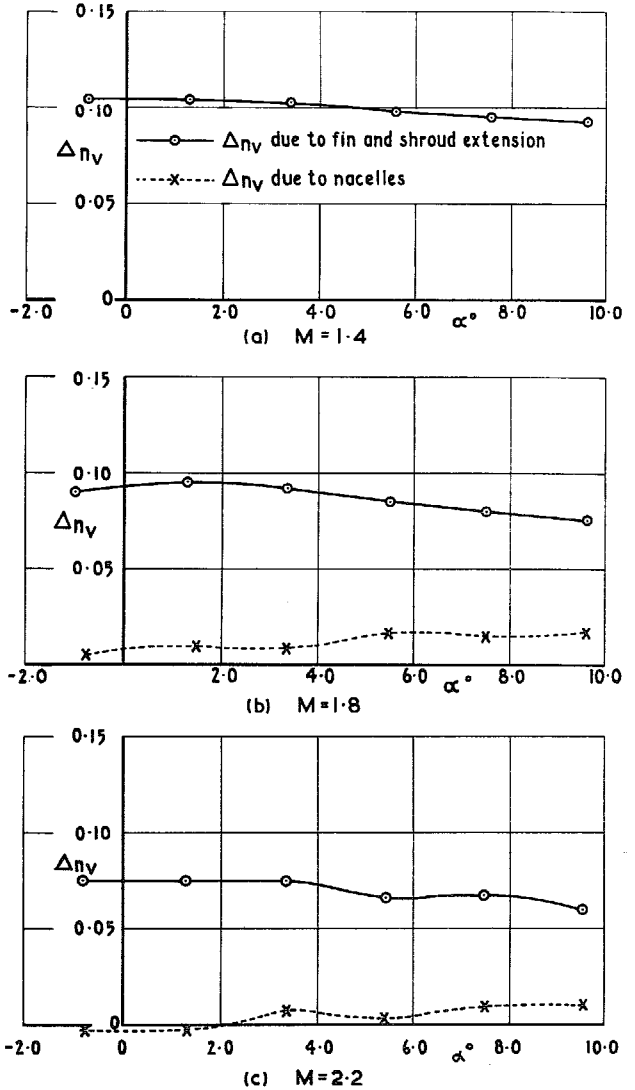

FIG. 56. Increments in n_v due to fin and nacelles at supersonic speeds.

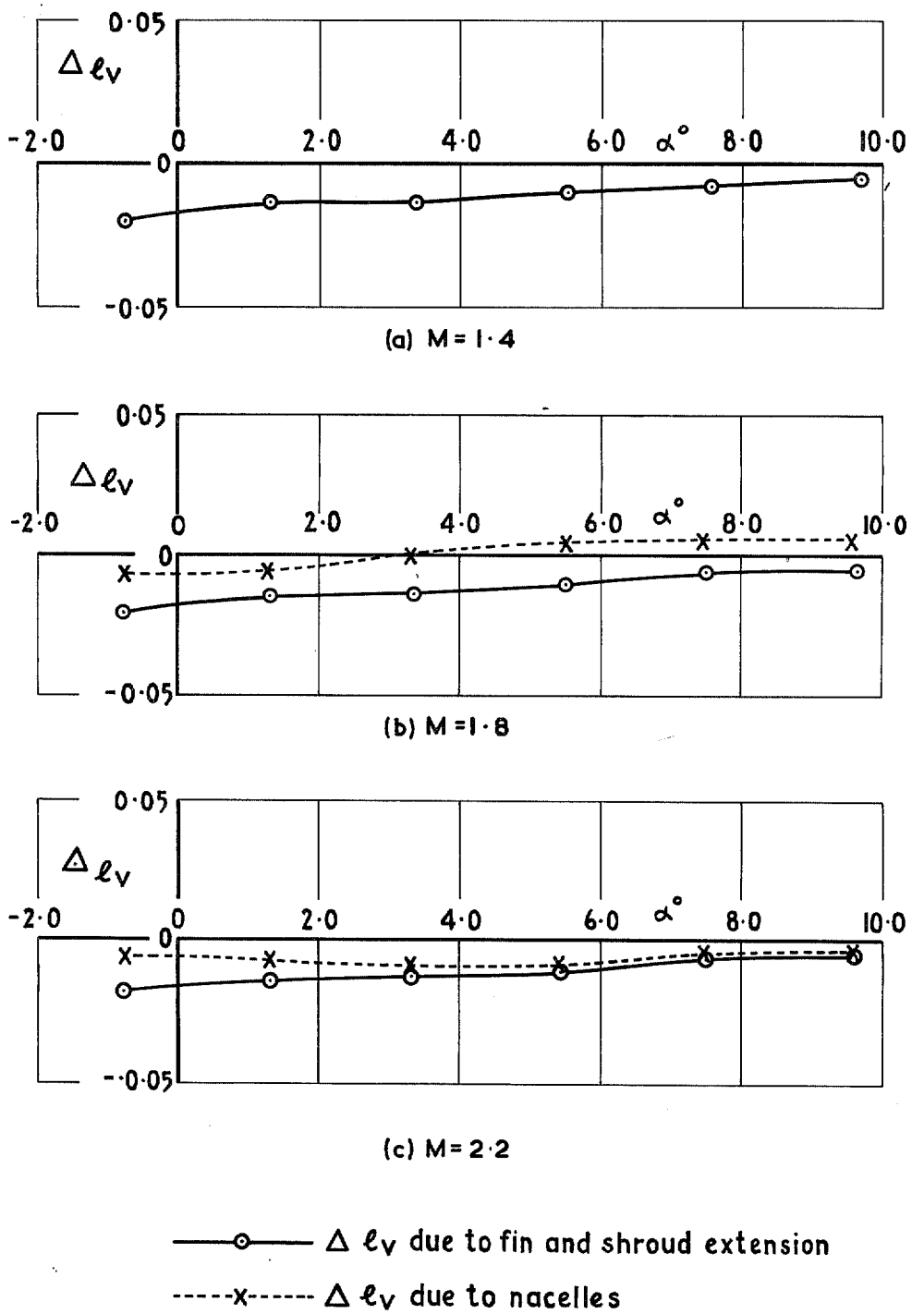

FIG. 57. Increments in l_v due to fin and nacelles at supersonic speeds.

Printed in Wales for Her Majesty's Stationery Office by Allens Printers (Wales) Limited

Dd. 135646 K.5

Published by
HER MAJESTY'S STATIONERY OFFICE

To be purchased from
49 High Holborn, London W.C.1
13A Castle Street, Edinburgh EH2 3AR
109 St. Mary Street, Cardiff CF1 1JW
Brazennose Street, Manchester M60 8AS
50 Fairfax Street, Bristol BS1 3DE
258 Broad Street, Birmingham 1
7 Linenhall Street, Belfast BT2 8AY
or through any bookseller

SBN 11 470190 3